12-18-2015

Pulsed Photonic Curing of Conformal Printed Electronics

Sourav Das
xd6026@rit.edu

Pulsed Photonic Curing of Conformal Printed Electronics

Sourav Das

Thesis submitted to the Faculty of

Rochester Institute of Technology

In partial fulfillment of the requirement for the degree of

Master of Science

in

Industrial and Systems Engineering

Department of Industrial and Systems Engineering

Date: 12/18/2015

DEPARTMENT OF INDUSTRIAL AND SYSTEM ENGINEERING

KATE GLEASON COLLEGE OF ENGINEERING

ROCHESTER INSTITUTE OF TECHNOLOGY

ROCHESTER, NEWYORK

CERTIFICATE OF APPROVAL

M.S. DEGREE THESIS

The M.S. Degree Thesis of Sourav Das
has been examined and approved by the
thesis committee as satisfactory for the
thesis requirements for the
Master of Science Degree

Approved by:

Dr. Denis Cormier, Thesis Advisor

Dr. Marcos Esterman, Committee Member

Abstract

As next-generation electronic products emerge, there is a need to create more electronic functionality in compact spaces. One of the techniques to achieve this is by integrating electronic circuitry on mechanical stress bearing parts of electro-mechanical products. Direct-write printing processes like inkjet printing and aerosol jet printing can be used to print conductive inks on conformal surfaces of mechanical components. Advanced curing/sintering processes such as pulsed photonic curing can be used to cure/sinter printed inks to produce conductive traces. However, the use of photonic curing on conformal surfaces introduces two sources of variability into the process, which are the distance and slope between the flash lamps and the conformal substrate. This research studies the effects that distance and slope between the flash lamps and substrate have on the characteristics of the photonically cured material. Screen printed samples of copper nanoparticle ink on paper substrates were photonically cured at various distances and slope settings in a Novacentrix Pusleforge 3300 machine. Analysis of the experimental data reveals that there is significant decrease in the conductivity of the cured copper ink with increase in both the distance and slope between the flash lamps and the substrate. The lowering of conductivity of the coupons with increase in distance was correlated to the reduction in the intensity of pulsed light with distance from the source. Similarly, the lowering of conductivity of the coupons with increase in slope was correlated to the reduction in the intensity of pulsed light with increase in angle between the incident light and the surface normal. A spectrophotometer was used to correlate the lowering of the conductivity of the printed coupon to the reduction in the amount of light absorbed by the coupon surface with increase in the slope from the flash lamps. This research highlights that distance and slope variations are important considerations to achieve uniform electrical properties in conformal printed electronics undergoing photonic curing.

Acknowledgements

Firstly I would like to express my most sincere gratitude to my advisor Dr. Denis Cormier for giving me the opportunity to work under him and for his continuous support, motivation and guidance. I have learnt a lot from him not only in the terms of research and academics but also discipline, perseverance and work ethics. I would also like to thank Dr. Marcos Esterman and Dr. Susan Farnand for their insights, support and guidance during the course of my thesis. I would like to express my gratitude towards the Industrial and Systems Engineering Department especially Marilyn Houck and Jennifer Barretta for their help and support over the last three years.

My lab mates Aakansha, Arjun, Chaitanya and Mike who made working in the Brinkman lab such a wonderful experience. My old friend and roommate, Pritam, for his enthusiasm, support and motivation.

Finally, I want to thank my parents Saswati and Kalyan Das for their constant support, love and faith. Without them this would not have been possible. A special thanks to Debjani for being with me through thick and thin.

There is only so many people I can name here, but I thank everyone who had made my stay at Rochester enjoyable and memorable.

Contents

List of Figures

List of Tables

Chapter 1 : Introduction

1.1 Integration of Mechanical and Electronic Components

As the next-generation of electronic products emerge, there is a need to create more electronic functionality in tighter spaces. Dedicated electronic circuit boards have traditionally been used to incorporate electronics into electro-mechanical assemblies. However, replacing the conventional electronic circuit boards and integrating electronics directly onto the mechanical part(s) can help save valuable space and reduce overall device complexity. The other obvious advantages are part consolidation, weight reduction, assembly time reduction and lower costs. Fabricating electronic circuitry on flexible substrates [1] and later molding them into 3D parts can help consolidate products. While, it is relatively easy to transform a 2D substrate into a cylindrical shape by flexing it about a single axis, it is difficult to flex sheet about multiple axes (e.g. hemispheres or saddle shapes) due to "puckering" effects of the sheet. Molded Interconnect Devices (MIDs) take an alternative approach towards integrating electronics, which are devised by using a plastic injection molded component and fabricating circuitry on its surface. A type of MID is fabricated using a two shot injection molding process, where two different polymers are bonded together to form a single part. One of the two polymers contains a special material, enabling it to be plated with a metal. However, bond strength and interface quality between the two polymers is an important challenge for this process [2], as are the environmental impacts of plating processes. Another method to produce MIDs is Laser Direct Structuring (LDS), where a thermoplastic doped with a metal plastic additive is used for injection molding the part. A laser then selectively etches the circuit pattern on the part followed by a metal coating process to form the circuitry [3]. But the limited number of available substrate materials restricts the application of this technique.

1.2 Additive Manufacturing

Additive Manufacturing/3D printing is the process of manufacturing a part directly from a digital model by depositing one layer of material on top of another. In the past, this process was mainly used for quick physical prototype fabrication during product development stages, giving it the name of Rapid Prototyping (RP). When the output quality of these machines is of sufficiently high quality that the resulting parts can be used in production, then the term Additive Manufacturing (AM) is used [4]. In AM, a Computer Aided Design (CAD) digital 3D model of the part is created and then sliced into numerous 2D profiles each having a specific thickness. Each 2D profile is sent to the 3D printer where each profile is printed on top of the previous one forming the final part. Figure 1 illustrates the basic steps involved in AM processes. The thinner the layer thickness and higher the printer resolution, the better will be the quality of the resulting 3D printed part. AM has the unique ability to manufacture near net shape products without the use of expensive tooling and multiple process steps, reducing the time to develop and market new products. AM is gaining popularity due to its ability to rapidly manufacture geometrically complex and custom low volume parts from a wide range of plastic materials like ABS, Nylon and PET [5]. Fused deposition modeling (FDM), Stereolithography (SL), Digital Light Projection (DLP) and Selective Laser Sintering (SLS) are among the commonly used plastic AM processes [4].

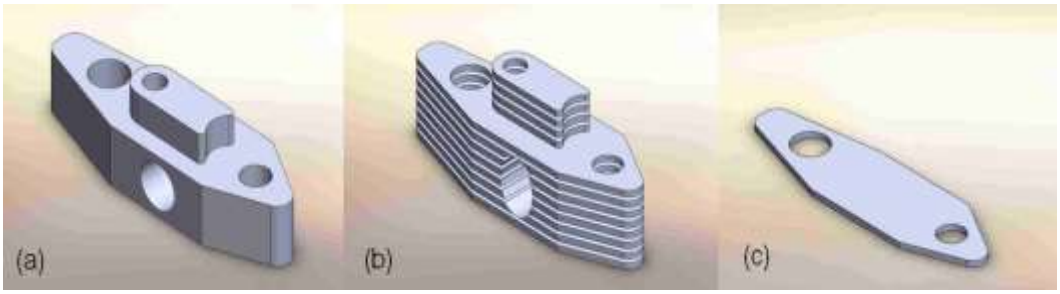

Figure 1: (a) Original CAD Model (b) Sliced CAD Model (c) First Layer Printed

1.3 Printed Electronics

The term “Printed Electronics” means the fabrication of electronic circuity, passive components and sensors by the means of conventional printing techniques on comparatively low temperature substrates like polymers, papers or fabrics. Traditional circuit board fabrication processes such as copper plating and etching have many processing steps and are seeing increased costs associated with potentially adverse environmental impacts. The development of revolutionary materials, large area printing processes, rapid curing techniques and mass customization are driving printed electronics deep into the commercial electronics market. The advantages of having low cost, fast processing times, high volume capacity and environmental sustainability are influencing electronics manufacturers to transition to printed electronics. The net revenue of printed electronics is estimated to be 30 billion USD in 2017 and 300 billion USD in 2028 [6].

Among the numerous printing processes associated with printed electronics, direct-write (DW) printing techniques are capable of printing functional electronic circuitry, passive components and sensors directly on flexible and conformal surfaces without any special tooling [7]. Generally, DW printers comprise of a CAD/CAM controlled print head dispensing an ink, which is mostly composed of metal nanoparticles suspended in a solvent or a liquid carrier. DW processes like continuous inkjet printing (CIJ) utilize a high ink dispensing velocity allowing them to print with larger stand-off distances. This enables CIJ to print on non-planer surfaces with a drop size of 100μm [8]. Aerosol Jet Printing (AJ) is a relatively new DW process. It uses nanoparticle ink mists and has the ability to print on conformal substrates with line widths as narrow as 10 μm [9].

In printed electronics, the ink printing process is followed by a subsequent curing process which sinters the metal/polymer nanoparticles together to form a continuous conductive

trace. Thermal curing [10], microwave curing [11], laser curing [12], electrical curing [13] and photonic curing [14] are among the common curing processes associated with printed electronics.

1.4 Multi-Material AM

In order to integrate mechanical and electronic components on the same part, a new multi-material AM process can be developed by combining existing methods of plastic AM and printed electronics fabrication techniques. Plastic AM processes can be used to fabricate mechanical stress bearing components, on which the electronic circuitry can be conformally printed using a DW printing process [15]. However, curing of the conformal printed traces on plastic parts is an important challenge to overcome in order to make this process viable.

One of the main challenges of multi-material AM is the ability to cure metal inks on plastic substrates. In the majority of multi-material AM research, silver ink or paste is most commonly used due to its relatively low curing temperatures (<150C) without any need for a protective or reducing atmosphere. Although silver is an excellent electrical conductor, it is an expensive metal. Copper is a good alternative to silver because of its high electrical conductivity, easy availability and lower costs. However, thermal curing of copper inks typically requires curing temperatures around at least 200C in order to achieve relatively good conductivity [16, 17]. It is impossible to heat most plastic AM parts to such high temperatures for any length of time because of their relatively low glass transition temperatures. ABS and PLA are among the most common plastics used in additive manufacturing having glass transition temperatures around 108C and 70C respectively. Moreover, thermal/oven curing of copper at temperatures around 200C can take up to a few hours, making the size of the ovens to be unrealistically long in a large volume printing

and curing operation. Laser based curing methods have been used to locally sinter printed inks; however, they hold the risk of damaging the polymer substrate [18]. Microwave radiation based curing methods have shown promising results; however, microwave conductors or antennas are required to absorb sufficient amounts of radiation to give decent ink conductivity. The additional requirements of printing of antenna patterns followed by oven sintering prior to other operations can make the microwave based curing impractical for high volume processing [19].

Pulsed photonic curing is potentially a good choice for high speed curing of conformal printed electronics because of its unique ability to cure metal/polymer inks without damaging the low temperature plastic substrate [20]. The advantages of micro-second processing times with a broad spectrum energy source makes it a potentially good candidate for conformal curing of DW printed inks on plastic AM parts. Photonic curing has been successfully integrated with roll-to-roll (R2R) printing processes for electronic component production [21]. Thus, plastic AM methods and DW printing processes coupled with pulsed photonic curing can help achieve the amalgamation of mechanical and electronic functionality in a single part leading to more compact and improved product designs.

1.5 Photonic Curing

Photonic curing is a relatively new curing technique used in the domain of printed electronics. In photonic curing, printed nanoparticle inks are cured using a high intensity broad spectrum light emitted from xenon gas filled flash lamps. This technology was pioneered and first introduced to the public in 2006 by Novacentrix of Austin, Texas [14]. In this process, the printed films of metal nanoparticle inks are passed under optimized high intensity light which optically cures the nanoparticle films without thermally

damaging the substrate. The primary advantage of photonic curing is that metal nanoparticle inks can be cured on relatively low temperature substrates like polymer or paper without damage to the substrate. The schematic diagram illustrating the photonic curing process is depicted in Figure 2.

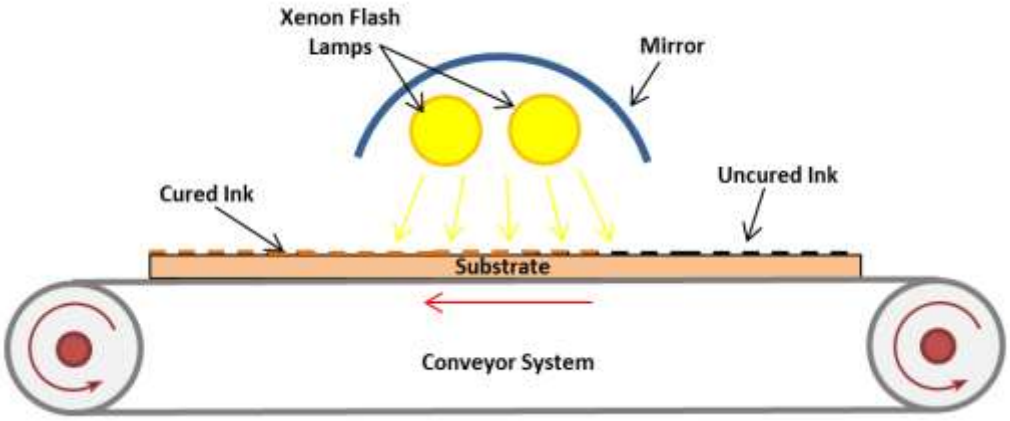

Figure 2: Photonic Curing Schematic [20]

1.6 Thesis Objective

The effectiveness of photonic curing for any given ink and substrate combination depends heavily upon on the power density (W/cm^2) of light exposure as well as the absorption spectra of the substrate. Lower power densities may partially cure a given ink, whereas excessively high power densities can ablate, or blow off, the ink. The lamp voltage, pulse length, number of pulses and pulse frequency of the Xenon lamps therefore need to be optimized in order to achieve good ink curing characteristics. However, photonic curing of conformal printed patterns introduce two new factors: the (1) distance between the lamps and the substrate, and (2) the angle between the incoming rays of light and the substrate. These two factors are illustrated in Figure 3. In Figure 3(a), the points A and B on the part are at different distances from the lamps but are both perpendicular to the direction of light rays. In Figure 3(b), points C and D are at the same distance from the Xenon lamps,

however, point C is perpendicular and point D is inclined at an angle θ° with respect to the direction of light rays.

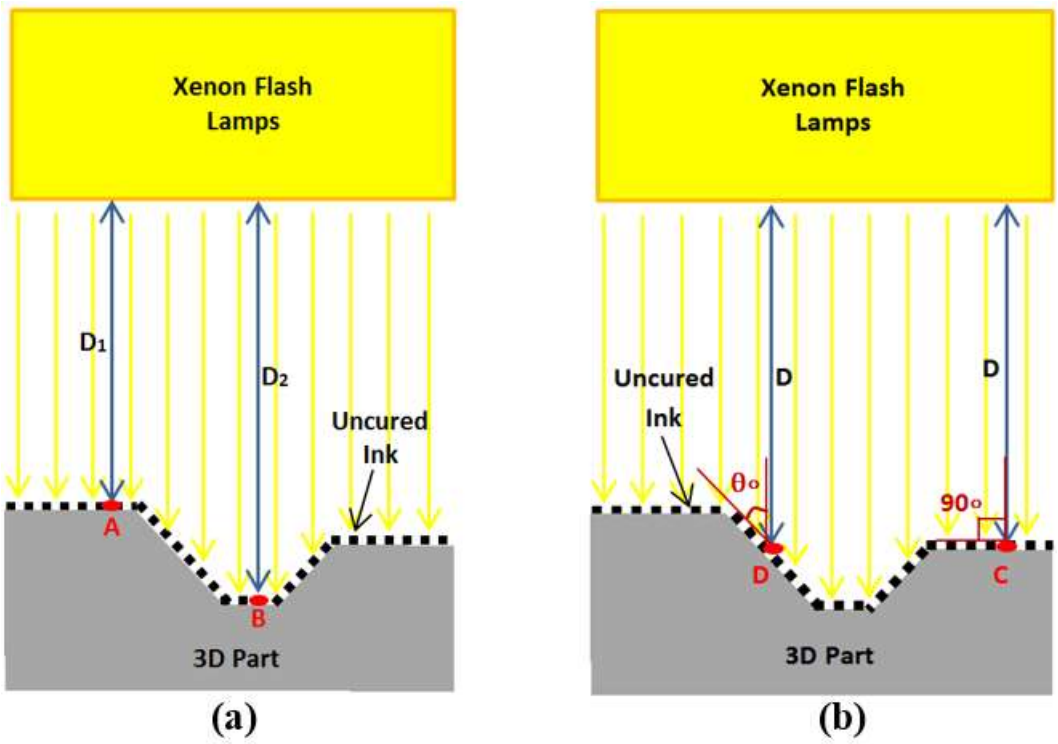

Figure 3: (a) Variation of Distance and (b) Variation of Slope during Conformal Photonic Curing

With these factors in mind, this research is focused on answering two fundamental questions regarding photonic curing of conformal electronics:

1. To what extent, if any, do variations in distance and slope during curing affect the quality of the printed nanoparticle ink?

2. If there are effects, what are the root causes, and how can they be overcome?

Chapter 2 : Literature Review

2.1 Conductive Inks

Both organic and metal conductive inks are widely used in printed electronics which are either solution, colloidal or suspension in nature.

2.1.1 Organic Inks

PEDOT:PSS is commercially available conductive polymer ink which can be both inkjet [22] and aerosol jet printed [23]. Graphene Oxide (GO) inks have been successfully inkjet printed to create gas sensors [24], flexible circuits and chemical sensors [25]. However, polymer inks typically have lower conductivity than metallic inks and may require an inert atmosphere during printing due to their high susceptibility to humidity and oxygen.

2.1.2 Metal Inks

Metal inks are often preferred over organic inks as they typically provide a better electrical conductivity. Metal inks can be prepared in two forms: metal nanoparticle (NP) inks and metal-organic decomposition (MOD) inks. NP inks are widely used as the nanoparticles can be easily produced in large quantities. But NP inks have a tendency to agglomerate over time, leading to settling and a short shelf life. MOD inks are typically in solution form, so they lack the tendency to agglomerate and clog the nozzle [26]. The nanoparticle inks are formulated with additives, such as dispersing agents and adhesion promoters that provide good printing properties by changing the ink viscosity and preventing the agglomeration of the nanoparticles. When a metal is in its nanoparticle form, there is reduction in its sintering or melting point [27]. This is particularly important, as it lowers curing temperature and time for NP inks, making the use of pulsed photonic curing on low temperature substrates possible.

Colloidal aqueous solutions of gold nanoparticles have been successfully inkjet printed with conductivities reportedly similar to that of bulk gold [28]. But gold inks cannot be used in mass scale electronics due to their high cost. Silver NP inks are an alternative to gold NP inks as they provide high conductivity at somewhat lower cost [29]. However, copper inks are of particular interest to the printed electronics industry due to their availability, lower cost, and excellent electrical properties. Low cost, high reliability and solderability are a few benefits of using copper inks [30]. Appropriateness of other metal inks like aluminum [31] has also been studied.

2.2 Printing Methods

Printing methods involved with printed electronics can be classified into two distinct categories: (1) contact printing where there is direct contact between the print head and the substrate, and (2) non-contact printing where there is no direct contact between the print head and the substrate.

2.2.1 Contact Printing

2.2.1.1 Screen Printing

In screen printing, a viscous ink is pushed through a screen mesh by a squeegee stroke onto a substrate. Masking of the screen mesh by polymer emulsion ensures selective coverage of the ink to form a specific pattern on the substrate. Although, screen printing has advantages like low cost, simplicity, and low wastage, the minimum printing resolution and speed is often limited to 100 μm and 30 m/min respectively [32]. However, screen printing is not suitable for printing on conformal surfaces. The schematic representation of the screen printing process is explained in Figure 4.

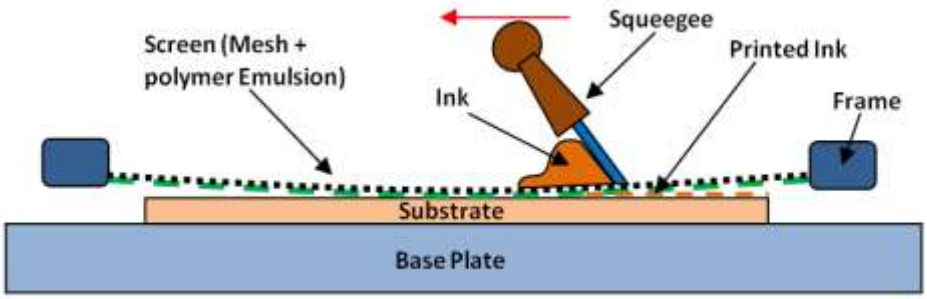

Figure 4: Schematic of Screen Printing Process [32]

For roll-to-roll (R2R) operations, a rotary screen printer can be used which increases the printing speed significantly [33]. The ink and the squeegee setup is place inside the rotary screen as illustrated in Figure 5.

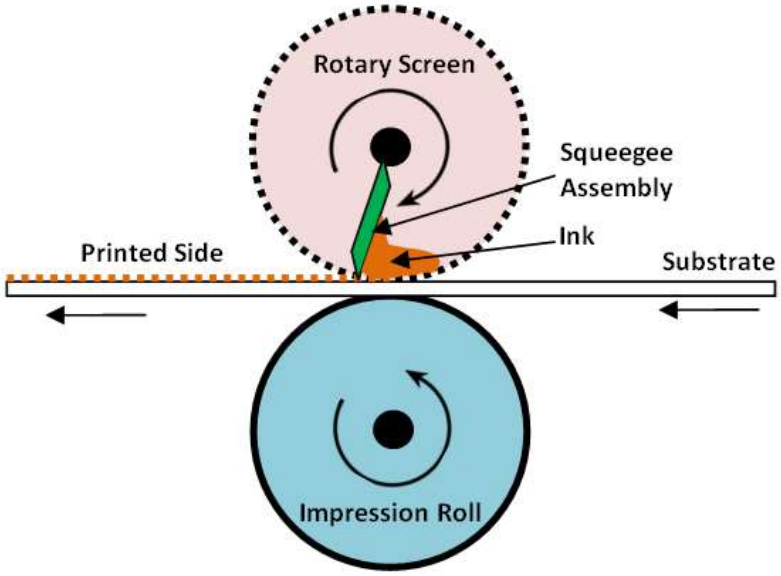

Figure 5: Schematic of Rotary Screen Printing Process. Adapted from [33]

2.2.1.2 Flexography

In flexography, ink is printed on the substrate by means of an embossed plate cylinder on which rubber/photopolymer plates containing the patterns are attached. Ink is supplied to the plate cylinder by the means of an Anilox roll; which is an engraved cylinder in which surface texture pick up ink from the bath. A tightly placed doctor blade scrapes off the excess ink from the anilox roll. The impression roll is used to adjust the pressure between the substrate and the plate cylinder. Although flexography is a rapid R2R process, patterns containing both large areas and fine features are difficult to print [33]. The schematic representation of the flexography process is depicted in Figure 6. However, flexography is not suitable for printing on conformal surfaces.

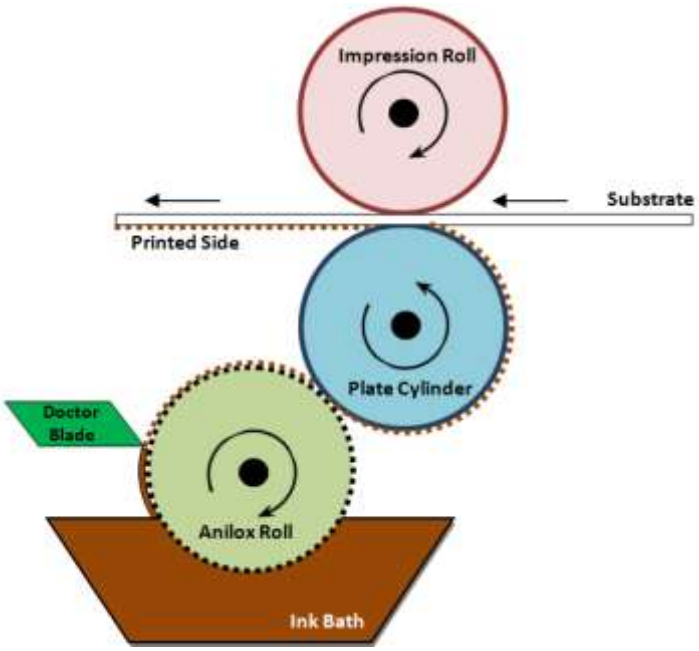

Figure 6: Schematic of Flexography. Adapted from[33]

2.2.1.3 Gravure Printing

Gravure printing is a well-established printing method in the printed electronics manufacturing industry. The qualities of having high resolution, ability to use low viscosity ink, wide range of film thickness and long term stability in high speed printing gives gravure printing its popularity. It has the ability to print on flexible substrates like paper and polymer films as well as rigid substrates like glass [34]. In gravure printing, the substrate is rolled between engraved cylinder and an impression roller. The engraved cylinder in dipped in an ink bath and a tightly pressed "doctor blade" scrapes off the excess ink before imprinting on the substrate [35]. Figure 7 gives the schematic description of the process. But gravure printing is not appropriate for printing on conformal surfaces.

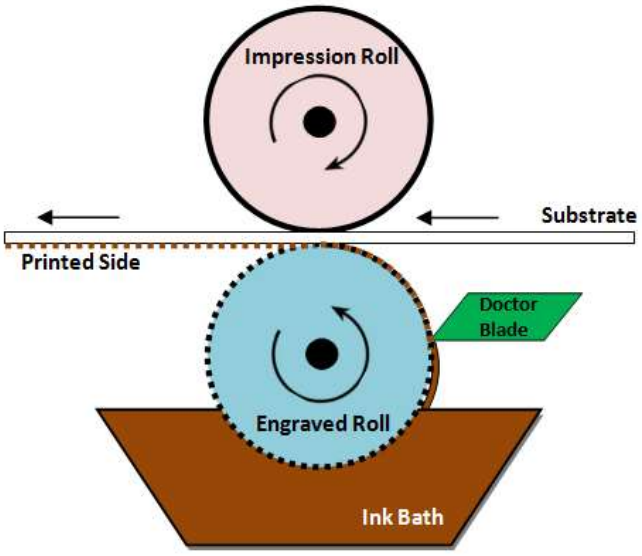

Figure 7: Schematic of Gravure Printing Process. Adapted from [34]

2.2.1.4 Gravure Offset printing

The gravure offset printing is a commercially successful printing method used by Samsung® and LG® for flexible electronics manufacturing [36]. The use of a highly viscous ink ensures the uniform dimensions of the printed patterns even after post processing. In the process, the ink is first doctored onto the grooves of the gravure plate. A silicon rubber wrapped metallic cylinder is generally used as the offset roller. The offset roller is rotated over the gravure plate with adequate pressure, picking up the ink from the grooves. Finally, rolling the offset roller over the substrates ensures the final printing. The greater the quantity of ink picked up by the offset roller, the better will be the printed result. The schematic for the plate-to-plate gravure printing process is shown in Figure 8. Although, the process seems complicated, using a gravure roll instead of the gravure plate can transform this process into a highly reliable R2R process [37]. A resolution of 67 μm has been achieved over multiple printing operations [36]. However, gravure off-set printing is not ideal for conformal electronics printing.

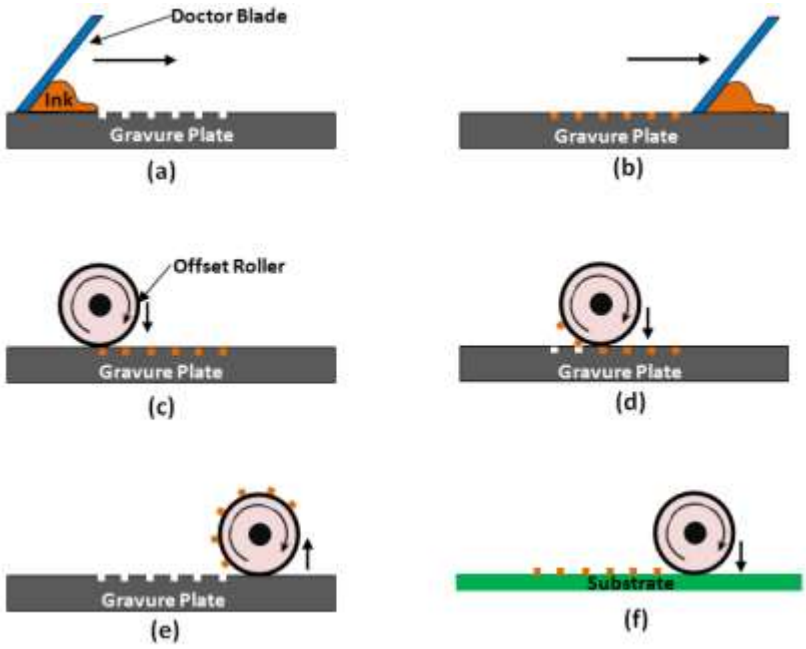

Figure 8: Schematic of Plate-to-Plate Gravure Offset Printing. Adapted from[37]

2.2.2 Non - Contact Printing

2.2.2.1 Extrusion-Based Printing

Extrusion-based DW printing uses a positive pressure to push a high viscosity ink through an orifice or nozzle onto a substrate. Control over the pressure is critical as it directly affects the feature width, even if the ink type and nozzle diameter are held constant [15]. Typically a syringe and plunger mechanism is used which is actuated by pneumatic or hydraulic pressure. A micro-extrusion system developed by nScript (Figure 9), uses a micro-dispensing pump, ceramic tip and syringe mechanism with precise pneumatic pressure control. It has the capability to print on conformal surfaces with a resolution in the hundred micron range [38].

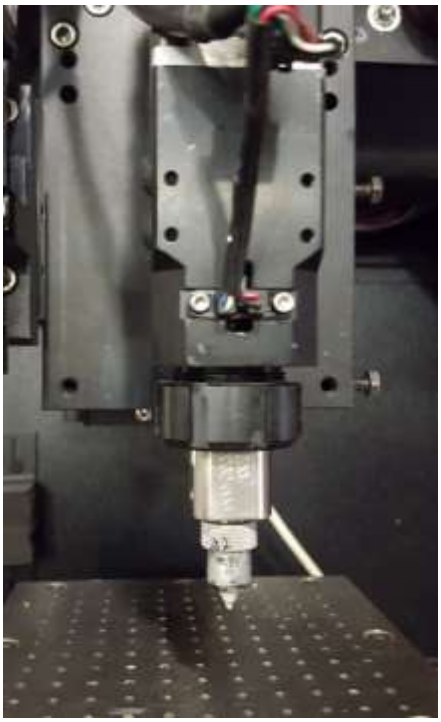

Figure 9: nScript Micro-dispensing Pump

2.2.2.2 Inkjet printing

Inkjet Printing is an immensely successful non-contact DW printing process, being widely used in office and home printers. Inkjet technology can be broadly classified into either continuous inkjet (CIJ) or drop-on-demand (DOD) categories.

CIJ is a more complicated method compared to DOD systems, making its use less common. In CIJ, a pump guides the ink into a small reservoir where a vibrating piezo crystal continuously ejects a stream of drops from the nozzle at a high frequency. The drops are acted upon by an electrostatic field which charges them and the deflection coils to determine the position where the drops will fall. The unused drops are collected and circulated back to the ink reservoir. The drops in CIJ fall at a rate of 25 m/sec, so a comparatively large distance can be kept between the print head and the substrate, which is advantageous in industrial environments. The large stand-off distance in CIJ gives it the ability to print over conformal surfaces within reason [8]. But CIJ has limitations in terms of low resolution and high maintenance requirements [39].

In DOD print heads, a pressure pulse in the ink reservoir ejects ink out of their nozzles only when they are required. DOD printers can be classified into thermal, piezoelectric and electrostatic, out of which the first two are most popular.

In thermal inkjet (Figure 10(a)), a current pulse is passed through a resistive heater placed inside the ink chamber near the nozzle. The heater vaporizes a small amount of ink, creating a bubble. The expansion of the bubble increases the volume of ink inside the chamber and forces it to come out of the nozzle. Then, as the current supply is switched off, the bubble collapses forcing the chamber to fill up with ink by capillary action [26].

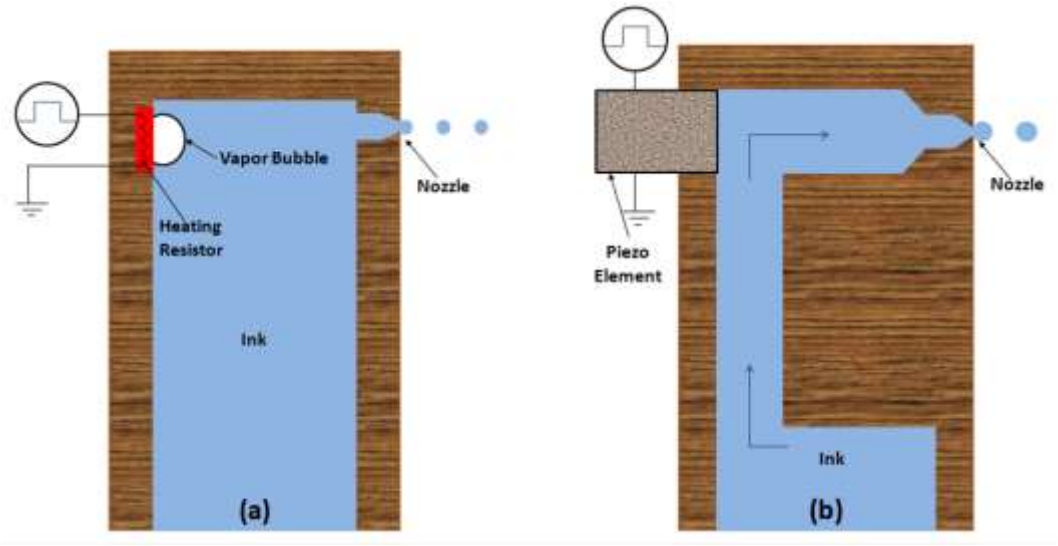

Figure 10: (a) Thermal Inkjet (b) Piezoelectric Inkjet. Adapted from [26]

In piezoelectric inkjet (Figure 10(b)), a piezoelectric element is placed inside the ink chamber. A voltage pulse passed though the piezo element forces it to expand and thus push out the ink through the nozzle. The amount and rate of the ink ejected can be easily controlled by manipulating the magnitude and frequency of the pulse [26]. This makes it a highly reliable print head with an immense flexibility over the ink formulations.

However, DOD inkjet printers are generally limited to use with extremely low viscosity inks and are not generally suitable for printing on conformal surfaces at low resolutions [15].

2.2.2.3 Aerosol Jet printing

Aerosol Jet (AJ) printing is non-contact DW process that deposits low or high viscosity inks on a wide range of 2D and 3D surfaces. Typical materials that can be printed are metal nanoparticle suspensions, conductive polymers and adhesives. As illustrated in Figure 11, AJ printing starts with the formation of an aerosol mist of the ink by the means of ultrasonic or pneumatic atomization. The aerosol mist is channelized through the nozzle where a co-

axial sheath gas aerodynamically focuses the stream. The aerosol jet print head is capable of focusing the stream to a width as narrow as 10μm using a 100 μm diameter nozzle [9]. The AJ print head is mounted onto a computer-controlled motion stage that determines where ink is printed. As the ink flow is continuous, a programmed shutter arm collects excess material when the system is not actually printing. The process, being computer controlled and non-contact, can be employed for printing over conformal surface with a stand-off distance of approximately 5mm [9].

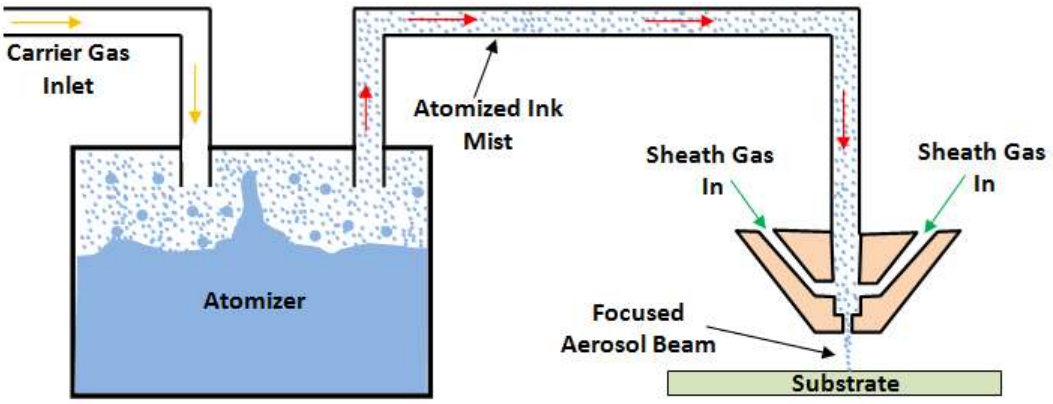

Figure 11: Aerosol Jet Printing. Adapted from [40]

2.3 Pulsed Photonic Curing – Pulse Forge 3300

Pulse Photonic Curing is a relatively new process in which printed films are cured using broad spectrum high intensity pulses from Xenon gas-filled flash lamps. This technology was pioneered by Novacentrix® of Austin, Texas and was first introduced to the public in 2006 [14]. The primary advantage of photonic curing is that metal nanoparticle inks can be cured on relatively low temperature substrates like paper, polymers and cloth usually without thermal damage. Other advantages of photonic curing are microsecond processing

times, independence with pattern size and the ability to process a wide range of materials. The dark color of most metal NP inks helps them to absorb light energy, and the high surface area to mass ratio of NP's allows them to heat up and cool down within a few microseconds. Simulations of the heat transfer process indicate that the NP's melt during the curing process and then rapidly cool before the heat is transferred to the substrate [41, 42]. Moreover, the phenomenon of melting point suppression also plays an import role in the photonic curing process which is described by the Gibbs-Thomson equation [27, 43].

$$T_M(d) = T_{MB}\left(1 - \frac{4\sigma_{SL}}{H_f \rho_s d}\right)$$

where T_M(d) is the suppressed melting temperature of the nanoparticle with diameter d, T_{MB} is the melting temperature of the bulk material, $\sigma_{SL}$is the solid-liquid interface energy, $H_f$is the bulk heat of fusion and ρ_s is the density of the solid material.

Figure 12: Pulse Forge 3300

The PulseForge 3300 is a commercially available pulsed photonic curing machine from Novacentrix® which can be integrated into a R2R process. It is capable of curing printed processing electronics at speeds that are generally in the range of 5-10 m/min. There are four primary control parameters with this process that can significantly affect the curing process:

- Pulse Voltage (V)
- Pulse Duration (μsec)
- Number of Pulses
- Pulse Frequency (Hz)

In order to get effective photonic curing characteristics for an ink and substrate combination, the above four parameters must be optimized.

2.4 Other Sintering/Curing Methods

2.3.1 Thermal Oven/Hot Plate Curing

Thermal curing using heated platens or ovens is one of the most reliable curing methods for nanoparticle inks. Initial heating of the printed patterns lead to the evaporation of the solvent, making the nanoparticles come in contact with each other. Subsequent heating leads to fusion and forms a continuous layer. A temperature of approximately 300°C is typically required to burn off most commonly used organic compounds completely [10]. However, inexpensive low temperature substrates such as polyethylene terephthalate (PET) cannot withstand these temperatures. If the curing temperature is lowered too much, incomplete combustion of the organics takes place, leading to an increase in the electrical resistance of the pattern [44]. Lowering of the curing temperature also increases the curing

time. Practically speaking, this leads to very long thermal curing ovens in a R2R process [14].

2.3.2 Microwave Sintering

Printed patterns of conductive metals like gold, silver and copper can be sintered using microwave radiation. The use of low temperature polymer substrates like PET is possible, as they are transparent to microwave radiation. This sintering method offers a fast, reliable and volumetric sintering of metal nanoparticle inks. Sintering times of around 240 seconds are required to yield about 5% of the bulk conductivity for silver inks [11]. However, antenna effects can improve the absorption of microwaves in printed patterns, dramatically reducing the sintering time to 1 second while yielding 34% of the bulk conductivity of silver [19]. But this requires additional printing of antenna patterns followed by oven sintering prior to other operations, which is not always feasible.

2.3.3 Laser Sintering

Laser sintering is a selective sintering method in which only the printed areas of a substrate are scanned with the laser. This is particularly useful when printed components contain several layers of different materials. Laser power and penetration depth can be adjusted to sinter different active material layers with different thickness. But as the time required to sinter is a function of the surface area of the printed traces, laser sintering is not always economical for large area electronics [12].

2.3.4 Joule heating

A freshly printed metal nanoparticle ink pattern usually has a high electrical resistance, which can be utilized for electric heating of the pattern. In resistance, or joule, heating, the flow of current through a highly resistive printed pattern leads to the generation of heat.

This heating leads to sintering or melting of nanoparticles to form larger grains with enhanced conductivity [13]. Joule heating can also be employed to improve conductivity of a previously sintered pattern [45]. Although joule heating is a fast process, high resistance of the printed pattern is prerequisite for the process. This precludes the use of metal organic decomposition (MOC) inks.

Chapter 3 : Research Methodology

3.1 Sample Preparation

In order to study the effect of distance and slope between the flash lamps and the substrate on photonic curing characteristics, sample specimens were prepared in order to carry out experimentation. Novacentrix Metalon ICI-021 aqueous dispersion copper oxide nanoparticle ink with 62% solid loading fraction was screen printed onto an A4 size (192mm x 262 mm) Wausau 110 lb paper substrate. A 280 mesh screen with a wire diameter of 25.4 µm (0.001 in.) and a 203 mm x 254 mm (8 in. x 10 in.) aluminum frame, was used to manually screen print the copper ink onto the paper using a squeegee mechanism. The complete manual screen sprinting setup is portrayed in Figure 13. Copper was chosen, as it is a conventional material for the fabrication of electronic circuits and PCBs.

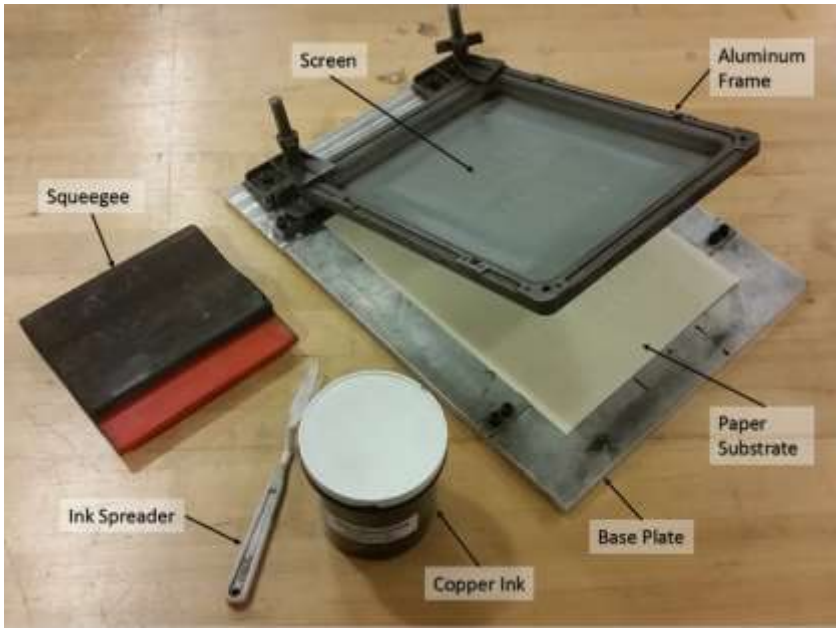

Figure 13: Screen Printing Setup

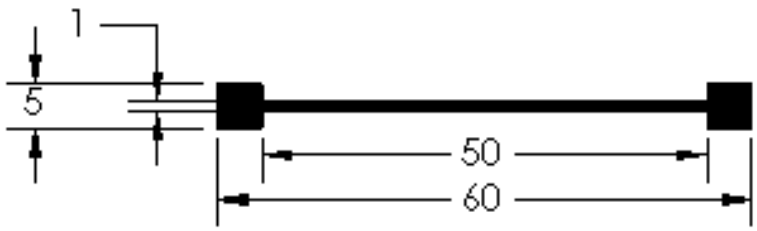

Figure 14: Printed Coupon Pattern (Dimensions in mm)

The pattern of the printed coupon is depicted in Figure 14. The pattern consists of a 50mm x 1mm line with two 5mm x 5mm square pads at the ends for taking conductivity measurements following photonic curing. Each manual screen printing cycle produced 16 identical printed coupons on an A4 paper sheet. Screen printing was chosen as the preferred printing method as it allowed printing of a large number of samples in a short duration of time, which could also be dried together prior to curing. This is particularly important, as preliminary tests indicated that drying time and temperature can be important factors contributing to the post curing conductivity. All of the printed coupons were simultaneously dried in an Across International Vacuum Oven VO-16020 (Figure 15) for 3 minutes at 150 ºC prior to photonic curing. The drying process helped in removing the organic solvents from the printed nanoparticle copper ink prior to photonic curing. After the drying cycle, each printed A4 sheet was cut up into 16 pieces each containing a single coupon, as shown in Figure 16. Each coupon was then cured separately in the Pulseforge 3300 during the experimentation phase.

Figure 15: Across International Vacuum Oven VO-16020

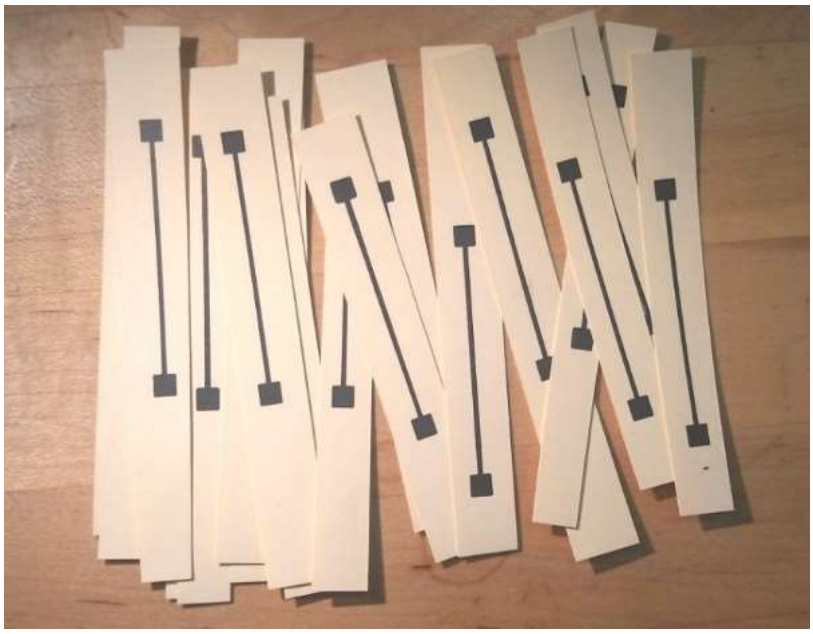

Figure 16: Coupons Ready for Undergoing Photonic Curing

The resistance across the cured coupon was used as the response variable to understand the effectiveness of photonic curing on electrical conductivity. The resistances across the cured test coupons were measured using a Fluke 115 TRUE RMS Multimeter (Figure 17).

Figure 17: Fluke 115 TRUE RMS Multimeter

The Novacentrix Metalon ICI-021 is an aqueous copper oxide NP ink that includes a reducing agent. During photonic curing, high intensity energy from the flash lamps initiates a reduction reaction in the printed coupon, removing the oxygen and leaving behind a fused copper film. As the carbon-based reducing agent is used up during the photonic curing process, it reacts to form rapidly expanding CO or CO_2 gas molecules that lead to a porous, or sponge-like, copper film. The micrographs of uncured and cured samples of Novacentrix Metalon ICI-021 copper ink are shown in Figure 18.

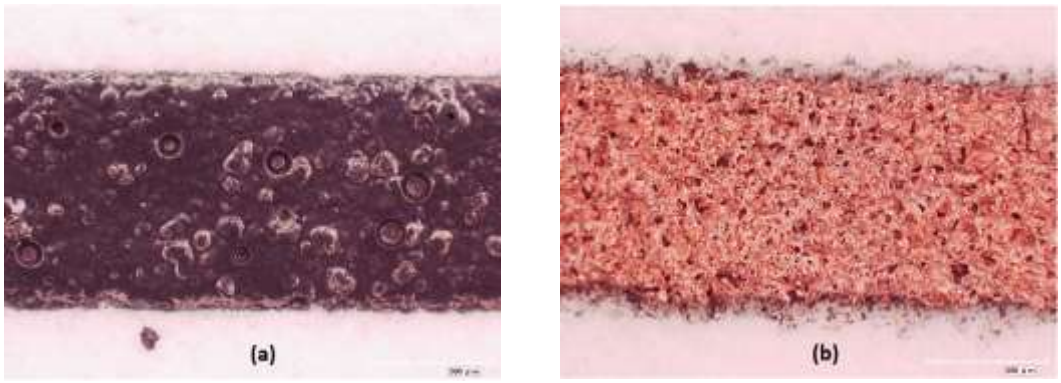

Figure 18: Micrographs of (a) Uncured and (b) Cured Samples of Novacentrix Metalon ICI-021 Copper Ink

3.2 Photonic Curing Parameter Optimization

In order to achieve the best possible conductivity for a printed ink, the photonic curing machine parameters need to be optimized for that particular ink and substrate combination. So before the distance and slope between the flash lamps and the substrate were varied to study their effects, the photonic curing parameters of Pulse Voltage (V), Pulse Length (μsec), Pulse Frequency (Hz) and the number of pulses (*n*) were optimized using a 2-step process for the Novacentrix Metalon ICI-021 copper nanoparticle ink and Wausau 110 lb paper substrate combination. Firstly, a trial and error method was used to bring down the 4 machine parameters within a small range. Later, a designed experiment was used to determine the final optimized parameter settings. Throughout the parameter optimization experiments, the distance and slope between the Xenon lamps and the substrate were kept constant at their standard (normal) positions, which were 17 mm (distance between lamp base and a fixed hard-stop point on the machine) and 0° (no slope) respectively. Also, the air knife inside the Pulse Forge 3300 was kept off throughout these experiments.

Pilot experimentation revealed that a single light pulse was not adequate to fully cure the copper ink. Similarly, using more than 2 pulses did not enhance the conductivity of the ink over what was obtained for 2 pulses. Thus from these results, it was concluded that 2 pulses were preferred for curing the Novacentrix Metalon ICI-021 copper ink and paper substrate combination.

A trial and error method was employed to vary the remaining 3 machine parameters of Pulse Voltage, Pulse Duration and Pulse Frequency with the objective of minimizing the resistance of the cured conductivity coupons. This method helped in bringing down the 3 machine parameters within a small range, which acted as the starting point for the parameter optimization design of experiments. The condensed parameter ranges obtained from the trial and error experimentation can be found in Table 1.

Table 1 : Photonic Curing Parameter Range Obtained from Trial and Error Experimentation

Curing Parameter	Parameter Range
Pulse Voltage	265 V – 275 V
Pulse Length	1300 μsec – 1400 μsec
Pulse Frequency	2.5 Hz – 3.0 Hz
No. of Pulses	2 Pulses

An experiment using Central Composite Design (CCD) was devised in Minitab to obtain the optimized parameter values from the condensed parameter ranges (Table 1). The 3 factors of Pulse Voltage, Pulse Duration and Pulse Frequency were incorporated in a Face-centered CCD experimental design having 8 corner points, 6 axial points and 6 center points. The experiment used 3 replicates, where each replicate was blocked and randomized within each block. Therefore, the total number of samples used was (8+6+6)*3

= 60. The experimental details and the data collected can be found in Table 2 and Appendix A respectively.

Table 2: Parameter Optimization DOE – Factors and Response Variable

Factors	**Low Level**	**High Level**
Pulse Voltage	265 V	275 V
Pulse Length	1300 µsec	1400 µsec
Pulse Frequency	2.5 Hz	3.0 Hz
Response Variable:	Resistance of coupon (Ohm)	
Replicates:	3	

The collected data was analyzed in Minitab®, and the main effects plots (Figure 19) were generated. The detailed output from Minitab® can be found in Appendix B.

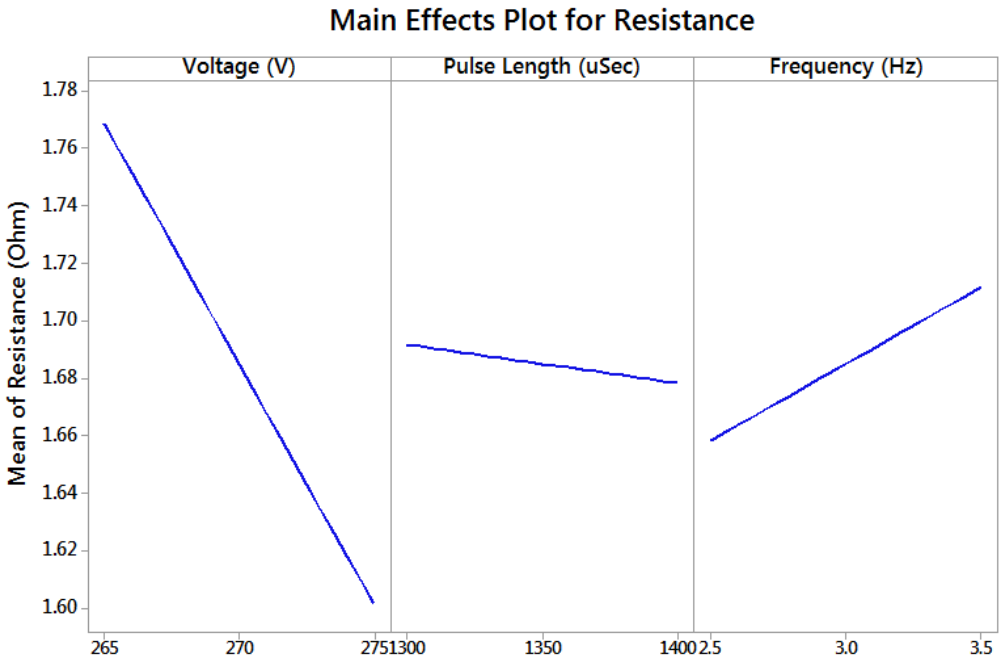

Figure 19: Main Effects Plot – Parameter Optimization.

The ANOVA table (Appendix B) reveals that within the specified range of the factors, voltage is the only significant factor with a low p-value (<0.05). However, the factors pulse length and frequency have high p-values (>0.05), and are thus considered insignificant. At 275V, the lowest resistance readings were obtained, hence this was set as the optimum value. Pulse length and frequency are insignificant factors, hence any choice of parameter value within the allowable range can be used. The values of 1370 μsec and 2.8 Hz were towards the lower end of the main effects plot of pulse length and frequency respectively. Thus they were chosen as the final optimized photonic curing parameters, summarized in Table 3.

Table 3: Optimized Photonic Curing Parameters

Curing Parameter	Parameter Range
Pulse Voltage	275 V
Pulse Length	1370 μsec
Pulse Frequency	2.8 Hz
No. of Pulses	2 Pulses

3.3 Distance and Slope Effect Study

In order to vary the distance and slope between the flash lamps and the printed coupons accurately, a set of fixtures were designed in Solidworks. The fixtures were fabricated by 3D printing them in ABS plastic using a Stratasys® Dimension Elite system. The set of fixtures shown in Figure 20 (a) and Figure 20 (b) were used to individually vary the distance and slope respectively. However, a combination of the two fixture sets could be used to obtain the exact of distance and slope requirements during the course of the experimentation.

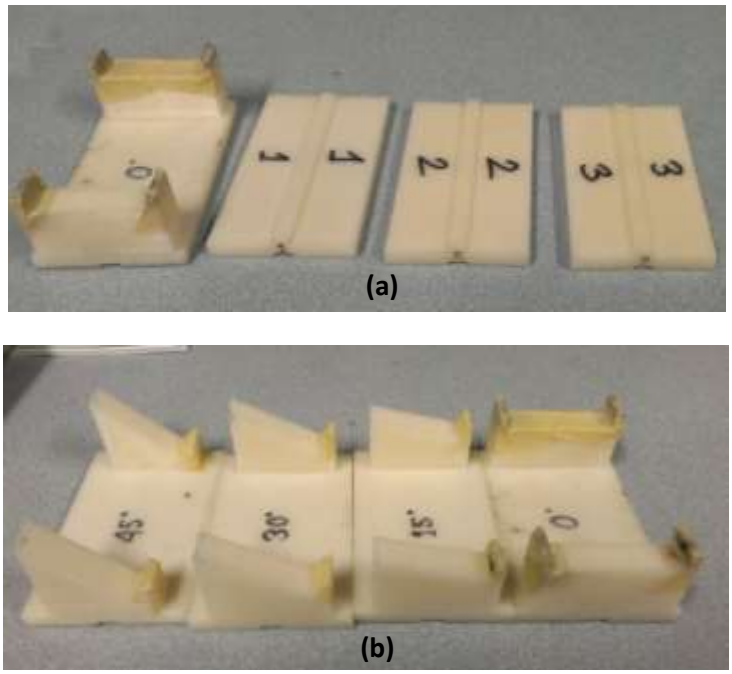

Figure 20: 3D Printed Fixtures to Vary the (a) Distance and (b) Slope

The individual printed coupons were first placed on a 3D printed ABS plate (30mm x 100mm) with the 50mm x 1mm line section of the coupon aligned along the center line of the plate. Two paper clips made sure that the coupon was securely locked at its position. This whole setup was then placed on top of the slope varying fixtures from the set shown in Figure 20 (b). The distance varying fixtures from Figure 20 (a) were placed below this setup in accordance to the height requirements. The step-by-step depiction of this process is illustrated in Figure 21. The variable slope fixtures were designed in such a manner that even if the slope of the coupon was changed, the distance of the 50 mm x 1mm line section of the coupon would always be at a constant distance from the base of the fixture. Additionally, in order to prevent the ABS fixtures from sustaining thermal damage due to repetitive photonic curing cycles, they were wrapped in aluminum foil.

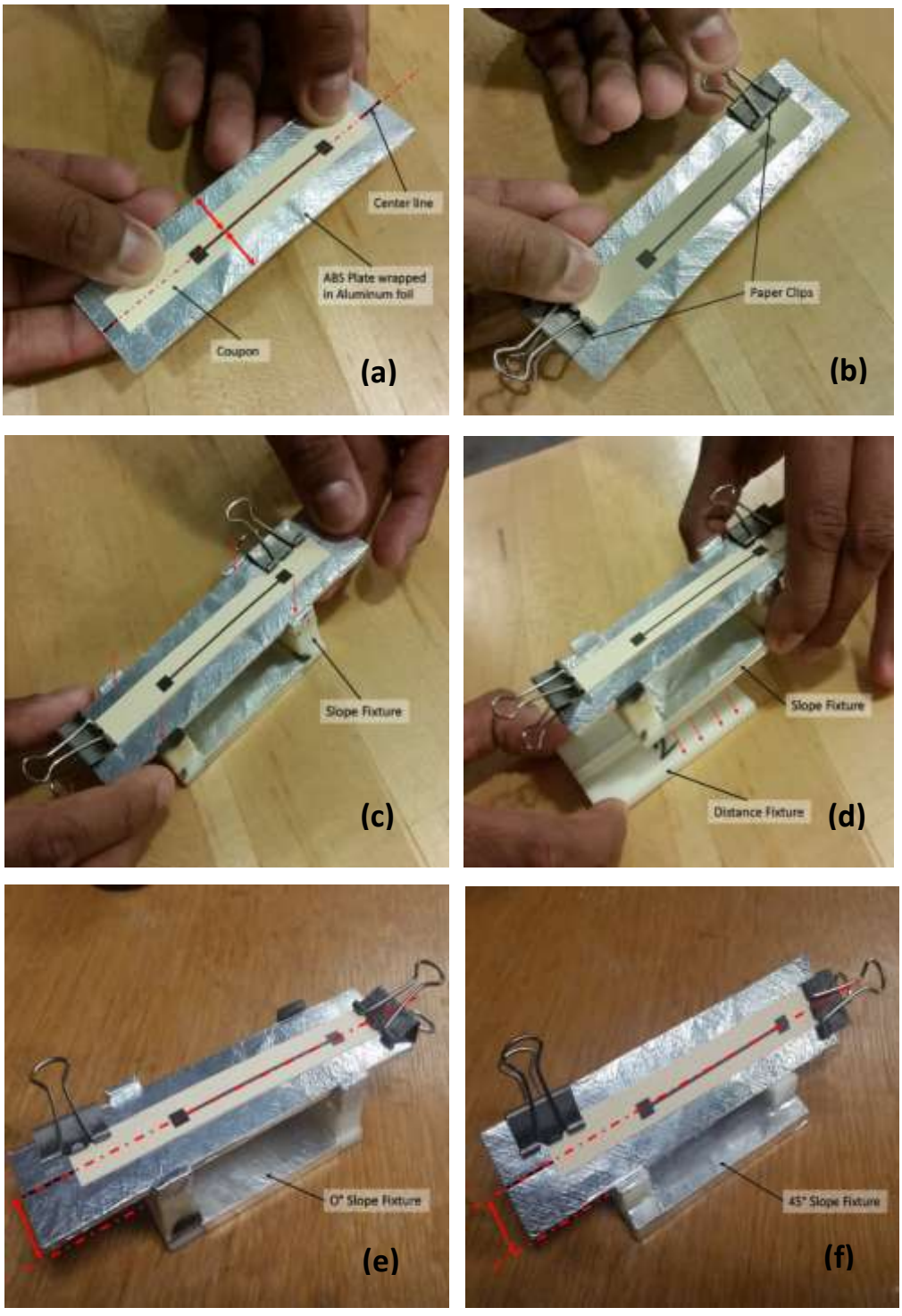

Figure 21: Steps Illustrating for Fixing the Printed Coupons onto the Fixtures

An experiment was designed in Minitab® taking the two factors of distance and slope at four different levels to study their effects. The four treatment levels of distance were 15 mm, 20 mm, 25 mm and 30 mm. The four treatment levels of slope were 0° (no slope), 15°, 30° and 45°. The photonic curing machine parameters used in this experiment were carried over from parameter optimization experiment tabulated in Table 3. These values were kept constant throughout the course of this experiment. Also, the air knife inside the Pulse Forge 3300 was kept off throughout this experiment. The experiment used 5 replicates, where each replicate was blocked and randomized within each block. Therefore, the total number of samples used was $4^2 * 5 = 80$. A significance level of 5% was considered for this experiment. The experimental details and the data collected can be found in Table 4 and Appendix C respectively.

Table 4: Distance and Slope Effect DOE – Factors and Response Variable

Factors	**Level 1**	**Level 2**	**Level 3**	**Level 4**
Distance	15mm	20mm	25mm	30mm
Slope	0°	15°	30°	45°
Response Variable:		Resistance of coupon (Ohm)		
Replicates:		5		

The experimental data was analyzed in Minitab® which suggests that there was a significant change in resistance of the printed coupons with change in both the distance and slope between the flash lamps and the sample. The detailed output from Minitab® can be found in Appendix D. The main effects plot in Figure 22 shows that the conductivity of the printed

samples decreases with the increase in both the distance and slope between the flash lamps and the substrate.

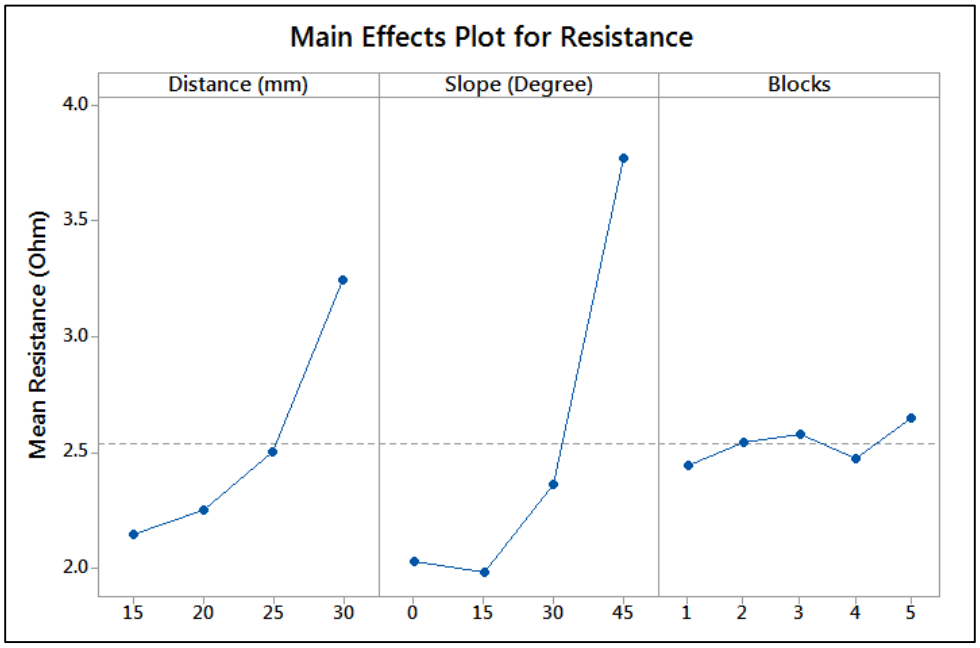

Figure 22: Main Effects Plot – Distance and Slope (Minitab® Output)

Analyzing the ANOVA table (Appendix D) revealed that there was significant blocking effect present as the p-value was 0.041 (<0.05). But comparing this to the p-values for the factors of distance, slope and their interaction effect show that the p-value for blocks is far larger. This is also confirmed by comparing the main effects plot in Figure 22. Thus, the effects associated with the factors of distance and slope are much greater than the blocking effect. The primary reason for the blocking effect to be significant is due to the presence of the multiple outliers in the data set shown in Figure 23 and Appendix D. This is likely because the manual screen printing process is not a very robust process and the printing is affected by factors such as the pressure applied on the squeegee and distribution of the ink on the screen.

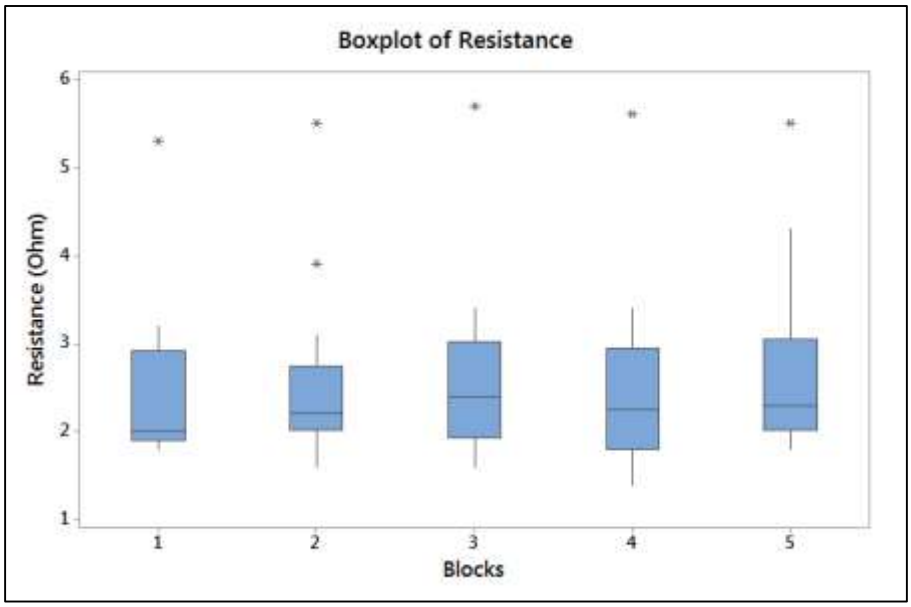

Figure 23: Boxplot of Resistance vs Blocks

The interaction plot in Figure 24 indicates that there is a significant positive interaction between the factors of distance and slope.

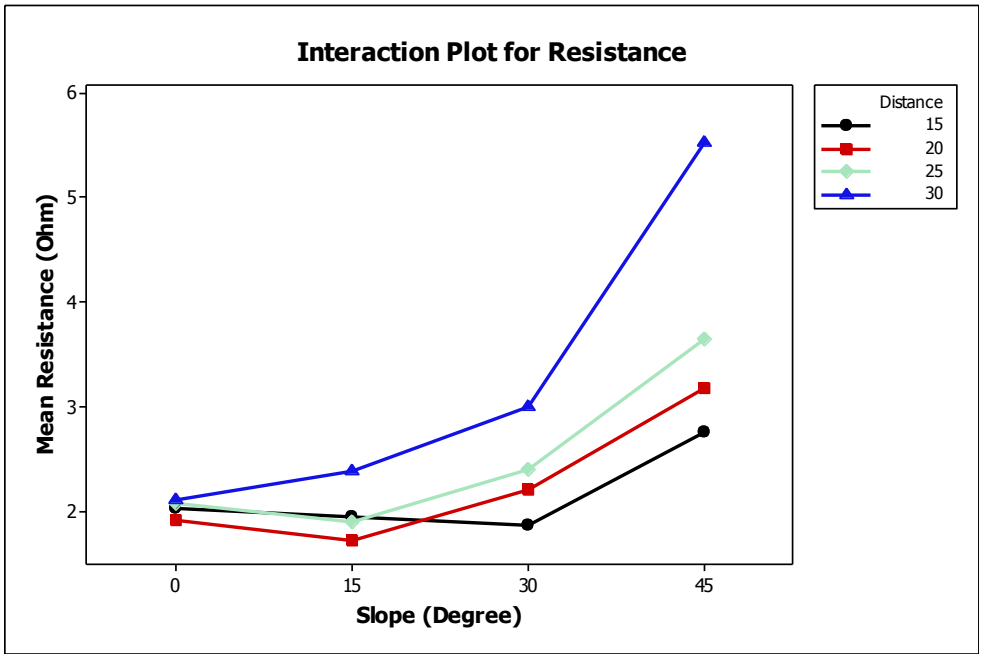

Figure 24: Interaction Effects plot – Distance and Slope (Minitab® Output)

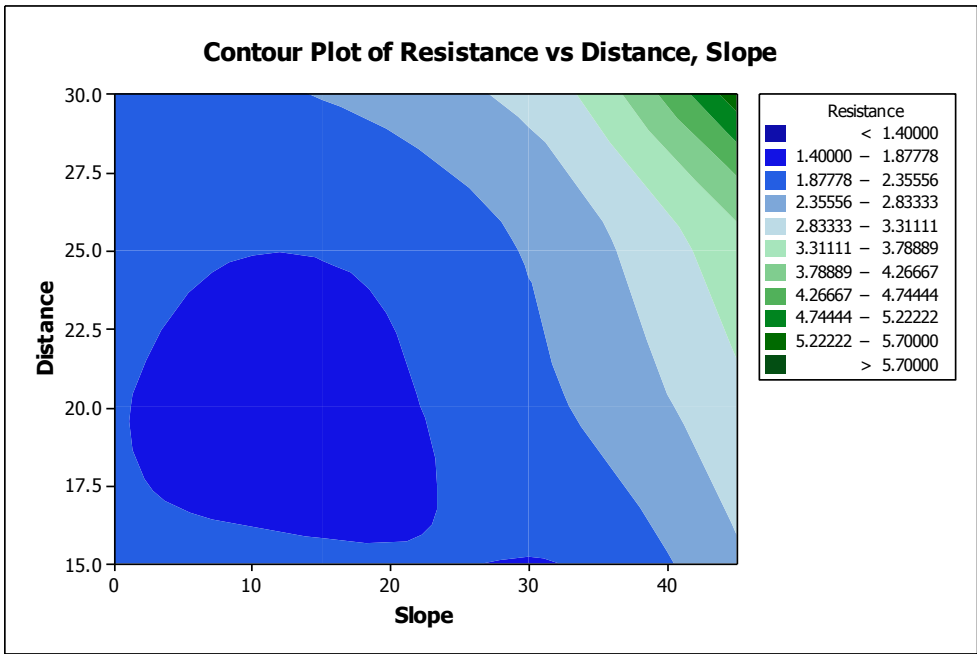

Figure 25: Contour Plot of Resistance (Ohm) vs Distance (mm) and Slope (Degree) (Minitab® Output)

The contour plot in Figure 25 shows the variance of the resistance of the coupons with respect to change in distance and slope.

The plots related to the residual analysis of this ANOVA are presented in Figure 26. From the normal probability plot, we can see that the points mostly fall on the straight line with only a few points shifting away from the line. Further, the histogram plot also describes a bell shaped normal distribution with mean at zero. Thus, the assumption of normal distribution of the residuals appears to be reasonable.

From the residuals vs observation order plot, no specific pattern is observed in the plot. Therefore, the assumption of the independence of the residuals appears to be reasonable.

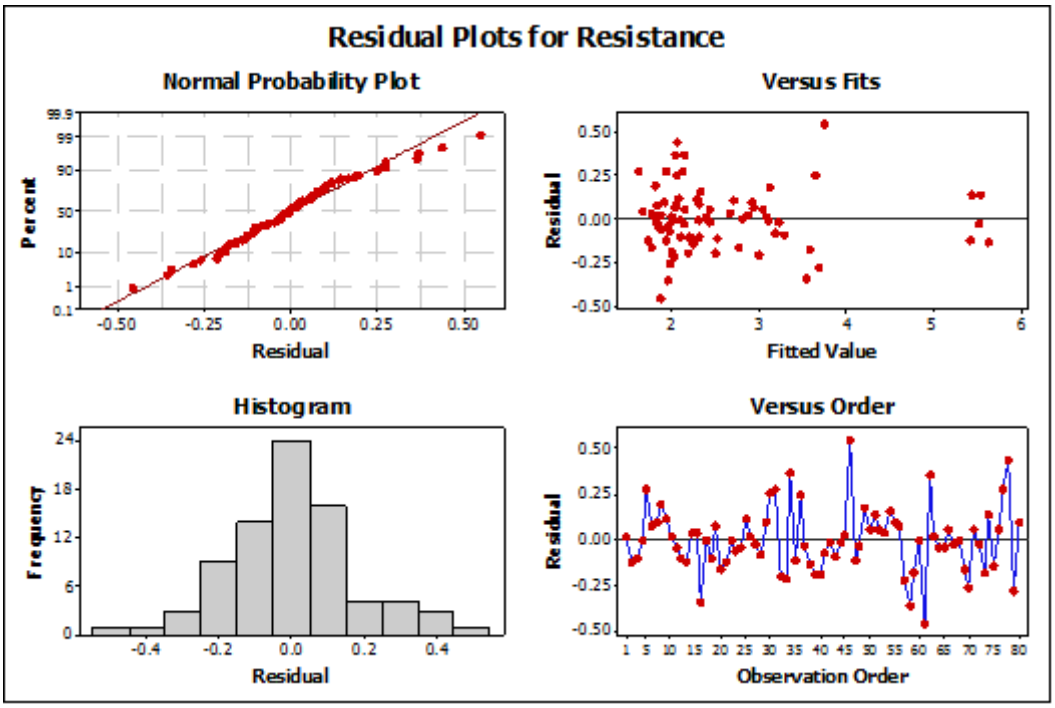

Figure 26: Residual Analysis Plots - Distance and Slope (Minitab® Output)

From the residual vs fitted value graph, it is observed that all the variances of the residuals have an approximate mean of zero. Therefore, the assumption of residuals being normally distributed with mean zero appears to be reasonable.

From the residual vs fitted value graph, it is observed that variances of residuals for the various fitted values are not equal. Therefore, the assumption of residuals being normally distributed with equal variance may be questionable. This is presumably due to the presence of outliers in the data set attributed to the manual screen printing process.

3.4 Distance Effect Modeling

In physics, the inverse square law of light states that the intensity of light at a point is inversely proportional to the square of the distance of that point from the light source. The inverse square law is defined by the equation

$$I \propto \frac{1}{d^2}$$

where I is the intensity of light/radiation commonly measured in Watt/cm^2 and d is the distance from the light source. The decrease in the conductivity of the cured coupons as distance between the flash lamps and the coupons increased was assumed to be due to the lowering of the light intensity in accordance with the inverse square law of light.

Figure 27: Novacentrix BX 100 Pulsed Light Energy Meter

To test this hypothesis, a Novacentrix BX 100 Pulsed Light Energy Meter (Figure 27) was placed under the exposure window of the Pulseforge 3300 to measure the light intensity at various distances from the Xenon lamps. An experiment was designed in Minitab where the single factor of distance was varied at 4 treatment levels which were 15 mm, 20 mm, 25 mm and 30 mm. For each distance level, the light intensity from the flash lamps was measured at 5 locations selected under the 127 mm x 76 mm (5 in. x 3 in.) exposure window shown in Figure 28. The experiment used 5 replicates, where each replicate was blocked and randomized within each block. Therefore, the total number of sample readings was 4 * 5 * 5 = 100.

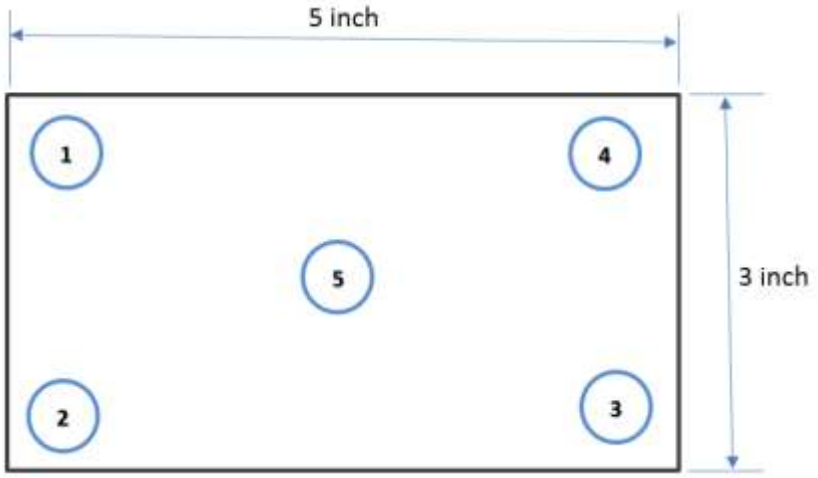

Figure 28: Pulse Forge 3300 exposure window

Throughout the experiment, the light intensity readings were measured using a single pulse of light generated using 275 V and 1370 μsec parameter values in the Pulseforge 3300 machine. As the output of the Novacentrix BX 100 Pulsed Light Energy Meter is given in units of energy density (J/cm2), the power density (W/cm2) can be obtained by dividing energy density by the pulse duration of 1370 msec. The experimental details and the data collected can be found in Table 5 and Appendix E respectively.

Table 5: Distance Effect DOE – Factors and Response Variable

Factors	**Level 1**	**Level 2**	**Level 3**	**Level 4**	**Level 5**
Distance	15mm	20mm	25mm	30mm	
Position	1	2	3	4	5
Response Variable:		Energy Density (J/cm^2)			
Replicates:		5			

The box-plot of the power density (W/cm2) at the 4 distance levels is presented in Figure 29.

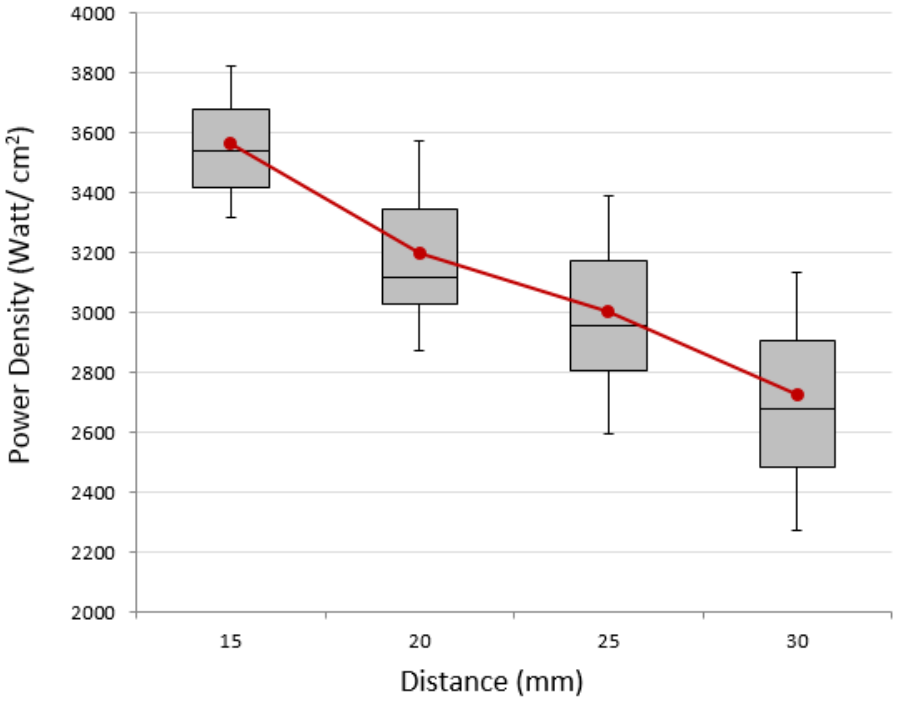

Figure 29: Box-plot showing the variation of power density (W/cm^2) at various distances from the Xenon Lamps

The experimental data was analyzed in Minitab® considering a significance level of 5% and is presented in Appendix F. The result suggests that there is a significant change in power density with change in the distance between the flash lamps and the light intensity meter. Thus, from the results of this experiment, it can be concluded that the lowering of the conductivity of the cured coupons with the increase in the slope between the flash lamps and the substrates was due to the reduction in the light intensity.

The main effects plot in Figure 30 shows that the light intensity decreases with the increase in distance between the flash lamps and the light intensity meter.

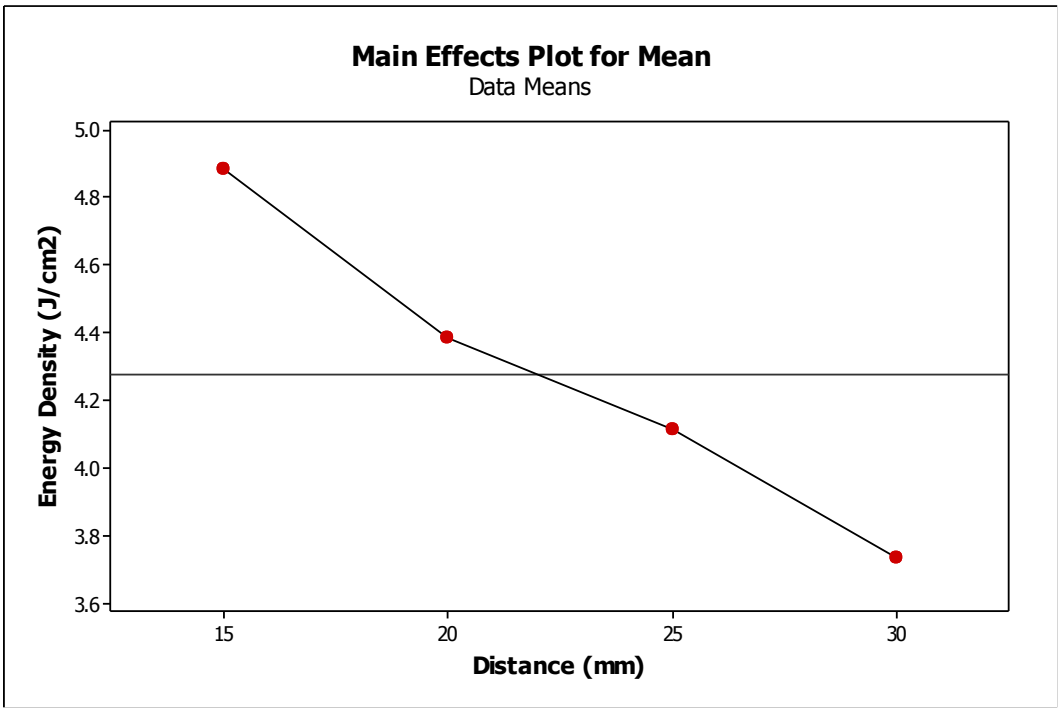

Figure 30: Main Effects Plot – Energy Density vs Distance (Minitab® Output)

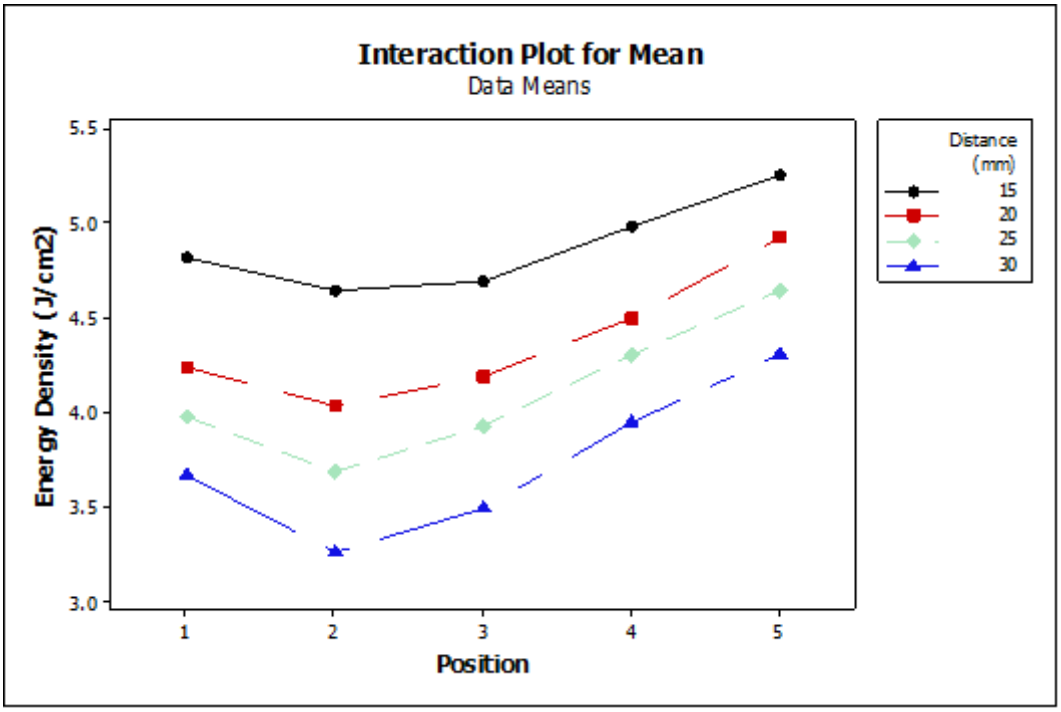

Figure 31: Interaction Plot – Energy Density vs Position vs Distance (Minitab® Output)

The interaction effects plot in Figure 31 reveals that there is significant difference between the observed light intensity between the 5 different locations under the exposure window for a constant distance from the lamps. One of the reasons for this phenomenon to occur can be the accumulation of depositions under the quartz plate that protects the lamps due to repetitive photonic curing of inks with volatile solvents.

The plots related to the residual analysis of this AVONA are presented in Figure 32. The normal probability plot reveals that almost all points fall on the straight line. Further, the histogram plot also describes a bell shaped normal distribution with mean at zero. Thus, it can be concluded that the assumption of normal distribution of the residuals appears to be valid.

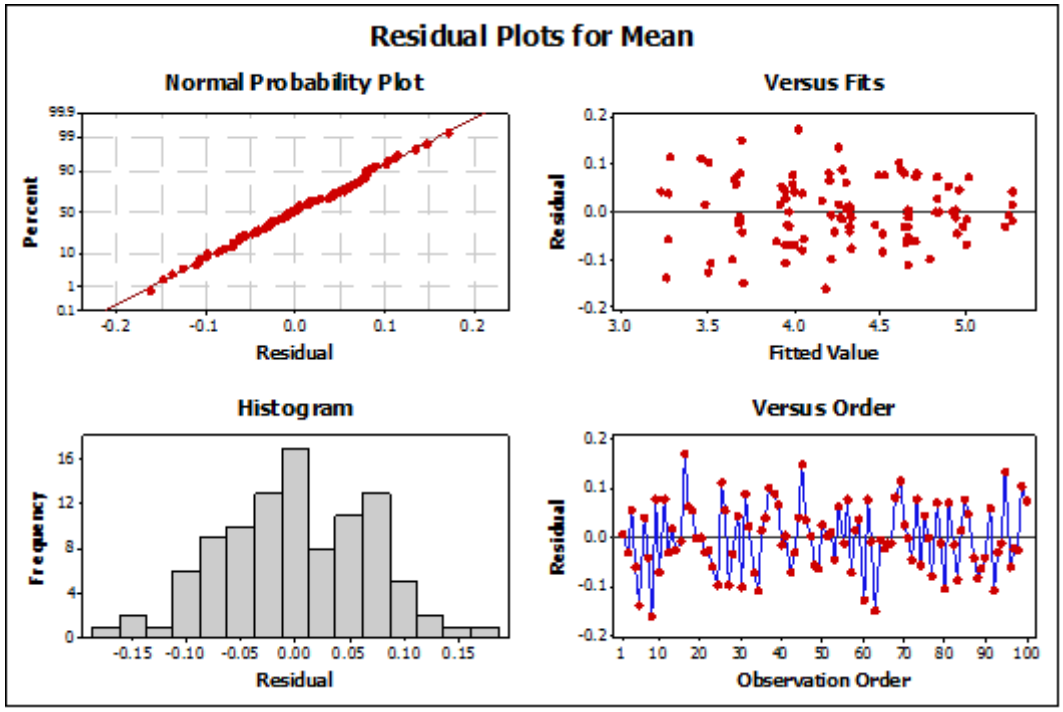

Figure 32: Residual Analysis Plots – Energy Density vs Distance (Minitab® Output)

From the residual vs fitted value plot, it was observed that all the variances of the residuals have an approximate mean of zero. Therefore, the assumption of residuals being normally distributed with mean zero appears to be valid.

From the residual vs fitted value plot, it was observed that variances of residuals for the various fitted values are approximately equal. Therefore, the assumption of residuals being normally distributed with equal variance appears to be valid.

From the residuals vs observation order plot, no specific pattern was observed in the plot. Therefore, the assumption of the independence of the residuals appears to be valid.

3.5 Slope Effect Modeling

The lowering of the conductivity of the cured coupons with the increase in the slope between the flash lamps and the substrate (Section 3.3) was assumed to be primarily due to the effect of the Lambert's cosine law. The Lambert's cosine law states that the luminous intensity of a surface is directly proportional to the cosine of the angle between the direction of light and the surface normal. This law is expressed by the equation

$$I_{surface} = I_{normal} \cos(\theta)$$

where I is the light intensity expressed in Watt/cm^2 and θ is the angle between the direction of incident light and the surface normal.

To test this hypothesis, a Novacentrix BX 100 Pulsed Light Energy Meter (Figure 27) was placed under the exposure window of the Pulseforge 3300 to measure the light intensity at various angles relative to incoming rays of light from the flash lamps. The variable slope fixtures (Figure 20 (b)) were used to vary the angle of the light energy meter. The arrangement of the entire setup is shown in Figure 33.

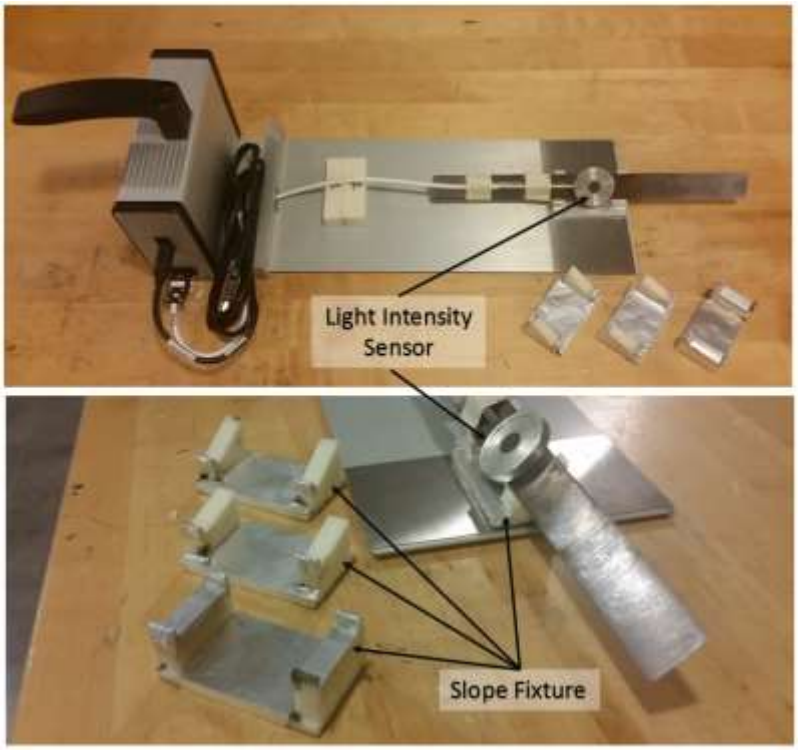

Figure 33: Novacentrix BX 100 Pulsed Light Energy Meter with Slope Fixtures.

An experiment was designed in Minitab® where the single factor of angle was varied at 4 treatment levels, which were 0°, 15°, 30° and 45°. The experiment was run with 10 replicates making the total sample observations to be = 4 * 10 = 40. A single flash of light was generated using parameter values of 275 V and 1370 μsec duration to take the individual light intensity measurements. Throughout this experiment, the distance of the light energy meter from the Xenon lamps was kept constant at a 17 mm. Power density (W/cm^2) was obtained by dividing energy density (J/cm^2) by pulse length. The box-plot of power density at the 4 angle levels is presented in Figure 34. The plots clearly show that the intensity of the light decreases with the increase in the slope between the flash lamps and the light intensity meter. Further, Figure 35 shows that the measured average power

density values match closely with the theoretical $I_{Surface}$ values. The experimental details and the data collected can be found in Table 6 and Appendix G respectively.

Table 6: Slope Effect DOE – Factors and Response Variable

Factors	**Level 1**	**Level 2**	**Level 3**	**Level 4**
Slope	0°	15°	30°	45°
Response Variable:		Energy Density (J/cm^2)		
Replicates:		10		

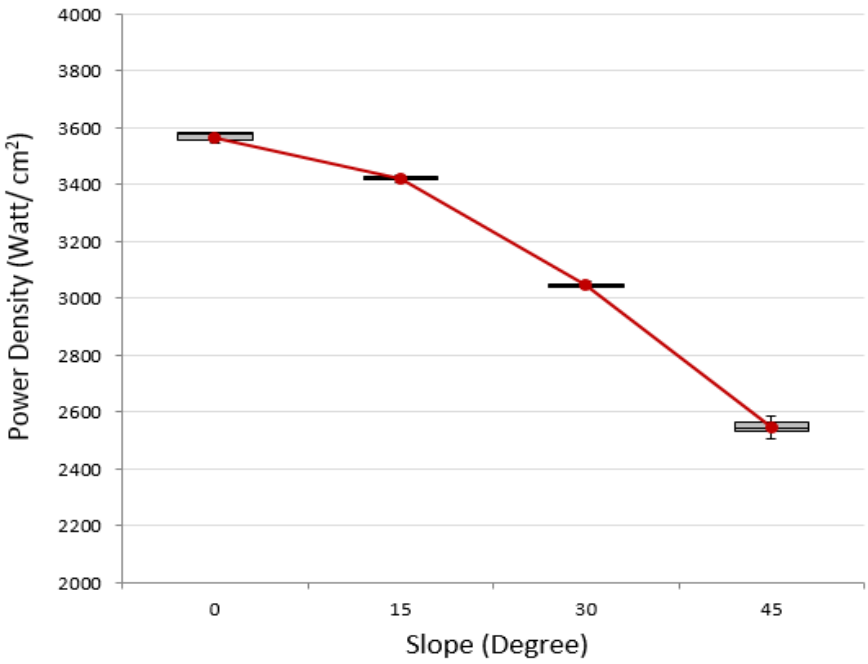

Figure 34: Box-plot Showing the Variation of Power Density (W/cm2) at Various Distances from the Xenon Lamps

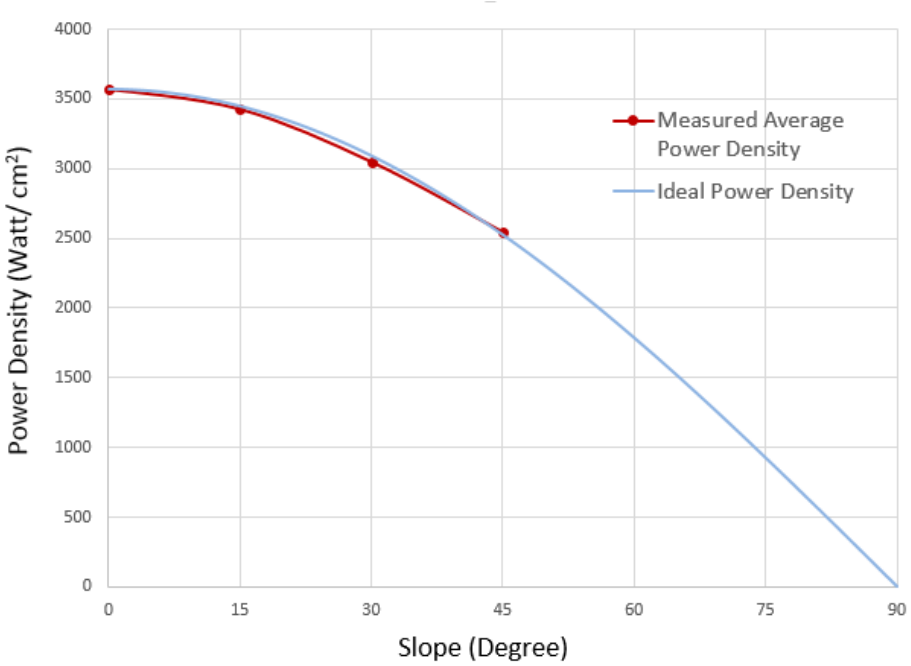

Figure 35: Ideal (I_{normal} Cos θ) Values VS Measured Average Power Density

Considering a significance level of 5%, the experimental data was analyzed in Minitab® which suggests that there is significant change in measured light intensity with change in the slope between the flash lamps and the light intensity meter. The Minitab output and the main effects plot for this experiment are presented in Appendix H and Figure 36 respectively. Thus, from the results of this experiment, it can be concluded that the lowering of the conductivity of the cured coupons with the increase in the slope between the flash lamps and the substrates was due to the reduction in the light intensity.

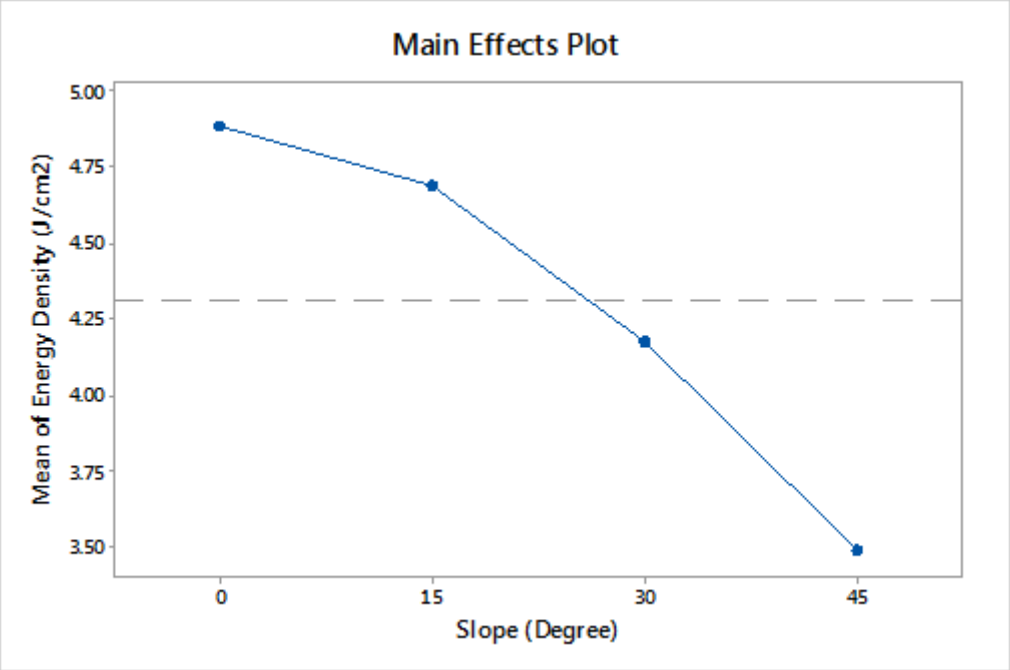

Figure 36: Main Effects Plot – Energy Density vs Slope (Minitab® Output)

The plots related to the residual analysis of this ANOVA are presented in Figure 37. The normal probability plot reveals that almost all points fall on a straight line. Further, the histogram also describes a bell shaped normal distribution with mean at zero. Thus, it can be concluded that the assumption of residuals being normally distributed appears to be valid.

From the residual vs fitted value plot, it was observed that all the variances of the residuals have an approximate mean of zero. Therefore, the assumption of residuals being normally distributed with mean zero appears to be valid.

From the residual vs fitted value plot, it was observed that variances of residuals for the various fitted values are approximately equal. Therefore, the assumption of residuals being normally distributed with equal variance appears to be valid.

From the residuals vs observation order plot, no specific pattern was observed in the plot. Therefore, the assumption of the independence of the residuals appears to be valid.

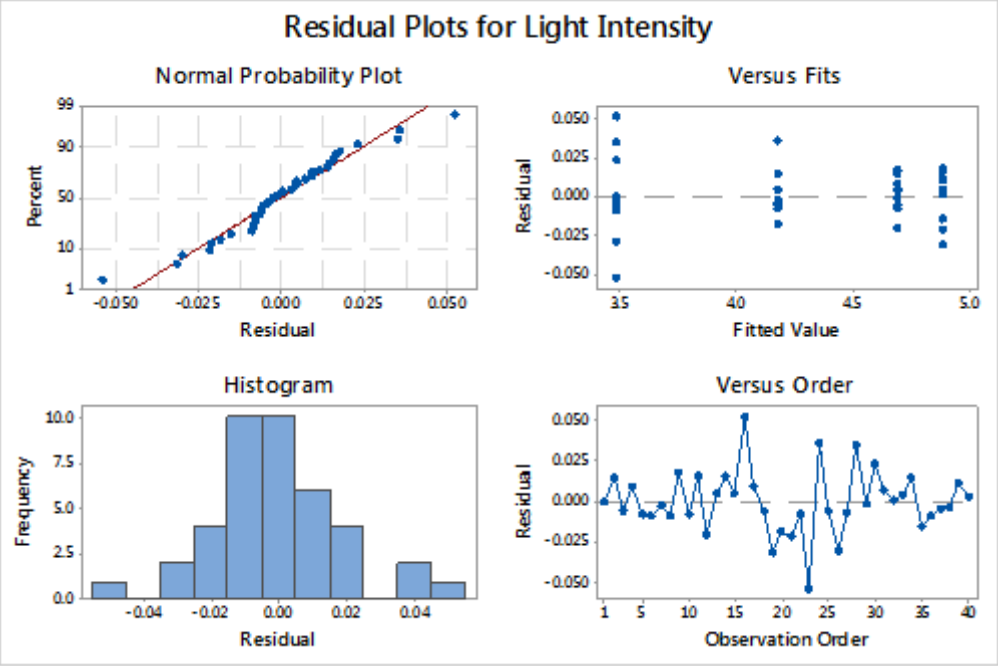

Figure 37: Residual Analysis Plots – Energy Density vs Slope (Minitab® Output)

The lowering of the conductivity of the cured coupons with increase in slope described in Section 3.3 was also assumed to be correlated to the decrease in the amount of light absorbed by the coupon surface. Theoretically, the total light energy falling on a surface is equal to the sum of the light energy absorbed, transmitted and reflected by the surface. Thus for a constant incident light source, the amount of absorbed light can be estimated if the amount of light transmitted through and reflected by an object is measured. To test this hypothesis, printed coupons were prepared similar to the ones described in Section 3.1.

To estimate the amount of light transmitted through the printed coupons, a Macbeth Color Eye® 7000 Benchtop Photospectrometer (Figure 38) was used. A printed coupon was placed inside the photospectrometer and was illuminated with a broad spectrum light. The amount of light transmitted through the coupon was determined by using the light receiving

sensor placed behind the coupon to collect the transmitted light. The collected data revealed that the amount of light transmitted through the coupon was negligible as expected for an opaque material. Thus, the light falling on the printed coupon could safely be assumed to be either reflected or absorbed by the coupon.

Figure 38: Macbeth Color Eye® 7000 Benchtop Photospectrometer

Figure 39: HunterLab® GCMS-10X Goniospectrophotometer

A HunterLab® GCMS-10X Goniospectrophotometer (Figure 39) was used to measure the light reflected off the printed coupon. The goniospectrophotometer gives its output in L* units which is the measure of perceived lightness of an object relative to the color in the scene perceived as white. The value of L* is generally between 0 and 100, where 0 indicates perfect black and 100 indicates white. L* is a dimensionless parameter which is defined by the equation

$$L^* = 116\left(\frac{Y}{Y_n}\right)^{1/3} - 16$$

where the term $\frac{Y}{Y_n}$ is the relative luminance of the object, and Y_n is the luminance factor for the scene white.

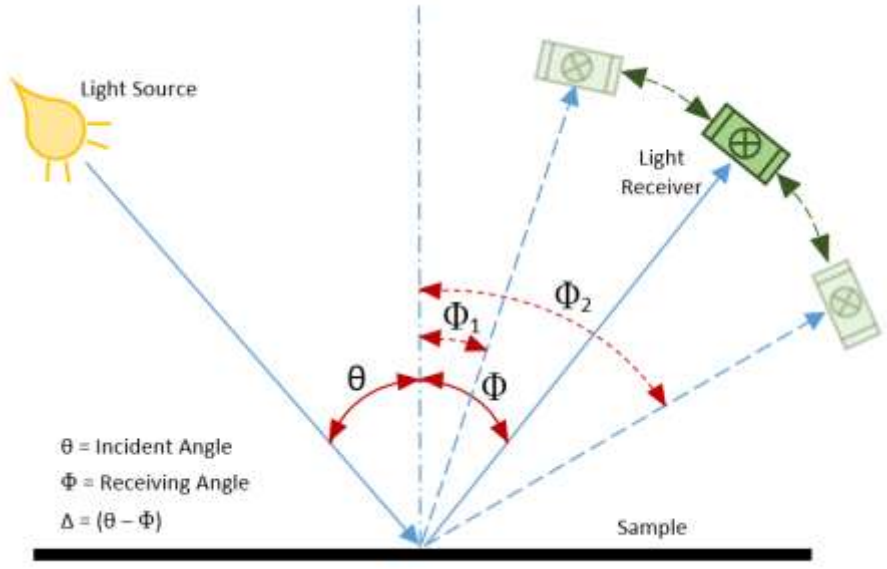

Figure 40: HunterLab® GCMS-10X Goniospectrophotometer process schematic

A printed coupon was placed inside the goniospectrophotmeter and illuminated with a broad spectrum light. The broad spectrum light was directed on the printed coupon at various incident angles (θ). For each incident light angle setting, the reflected light was

collected at various receiving angles (Φ) by revolving the light receiving sensor over the entire envelop. The schematic of this process is depicted in (Figure 40).

The L* data collected (Appendix I) for the various incident light angles (θ) was analyzed and plotted in MS Excel, which is shown in Figure 41. In Figure 41, the X-axis represents the value Δ (delta) which is the difference between the incident angle (θ) and the receiving angle (Φ). The Y-axis contains the computed L* value from the light readings. Although the metric L* does not directly measure the intensity of the reflected light, it can be correlated to the amount of light reflected by a surface as L* is a function of Y, which is a function of reflectance. Simply put, the lighter the color of the surface, the more light is reflected by it. Therefore, as more light is reflected by the surface, the L* value increases. Note: As it is difficult to place the light source and receiver sensor at the same physical location (refer Figure 40), L* data point values are absent between Δ -20˚ and + 20˚ for the 0˚ incident angle.

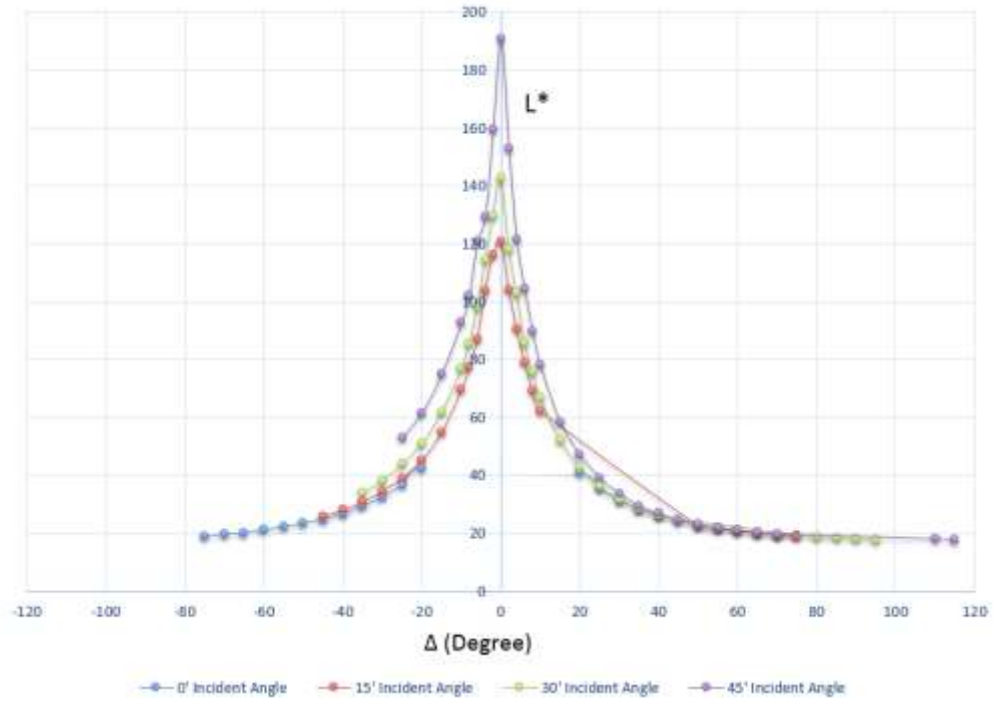

Figure 41: Delta vs L* Plots for Various Incident Light Angles.

The plot in Figure 41 reveals that with the increase in the incident light angle, the area under the L* curve increases. This signifies that as the incident light angle increases, the amount of light reflected over the entire envelope also increases. In Figure 41, it is observed that some of the L* values are more than 100, this is due to retro-reflection. Although it was not possible to exactly quantify the intensity of the reflected light, it can be concluded that the intensity of reflected light increased with increase in the incident light angle due to the fact that L* is proportional to the reflectance. From the results of this experiment, it can be concluded that the lowering of the conductivity of the cured coupons with the increase in the slope between the flash lamps and the substrates is also partially due to the decrease in the amount of light absorbed by the coupon surface.

Chapter 4 : Conclusions and Recommendations

4.1 Summary

The research proposes the idea of incorporating plastic additive manufacturing and conformal printed electronics into a single multi-material process to produce electro-mechanical components. This process will help assist manufacturing of the next generation consumer electronics with more functionality in constricted spaces. Photonic curing is bound to play an important role because of its ability to cure conformal printed electronics without thermally or chemically damaging the underlying plastic part.

This thesis describes the effect distance and slope between the xenon flash lamps and the substrate will have on the electrical properties of photonically cured conformal electronics. Experimental results revealed that there was significant decrease in the conductivity of the printed coupons with increase in both the distance and slope between the xenon lamps and the substrate.

A Novacentrix BX 100 Pulsed Light Energy Meter placed in the Novacentrix Pulseforge 3300 was used to measure the light intensity at various distances from the flash lamps. The experimental results revealed that the light intensity lowered with the increase in the distance between the sample and lamp unit, which can be associated to the lowering of the conductivity of the cured coupons.

The Novacentrix BX 100 Pulsed Light Energy Meter was also used to measure the light intensity at various angles with respect to the incoming light beams. The collected data showed that the light intensity lowered with the increase in angle between the incident light and the surface normal of the light intensity meter. This was correlated as the primary reason for the lowering of the conductivity of the cured coupons. Further, a HunterLab®

GCMS-10X Goniospectrophotometer was used to measure and compare the light reflected by the copper ink surface for various incident light angles. The results revealed that with increase in the incident light angle, the amount of light absorbed by the copper ink surface decreases. This was also correlated to the decrease in the conductivity of the cured coupons.

In summary, this paper points out that distance and slope variations are important considerations to achieve uniform electrical properties for conformal printed electronics undergoing photic curing.

4.2 Recommendations for Future Work

This research identifies that there can only be a limited amount of variation in the height and slope of a conformal printed part undergoing photonic curing in order to have uniform electrical characteristics. One of the methods to overcome this problem is by reorienting the parts inside the photonic curing machine and then repulsing on the partially cured areas again. This process is briefly described in Figure 42.

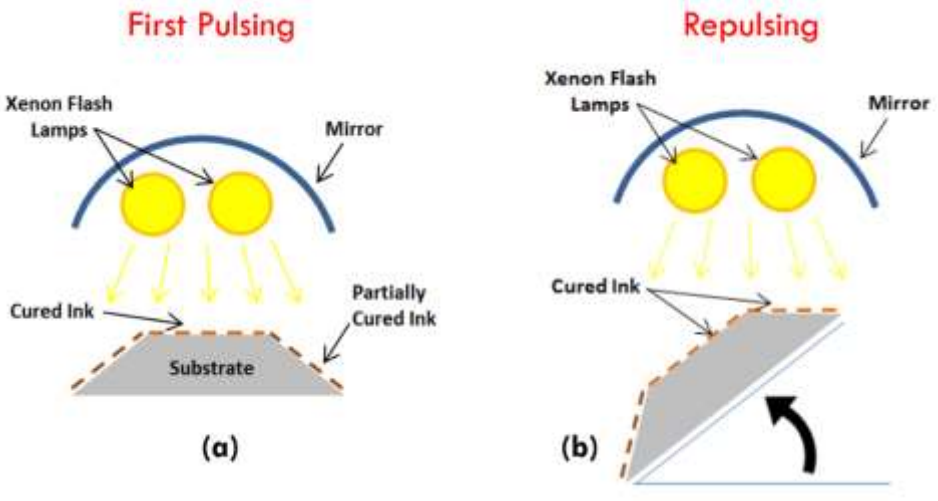

Figure 42: (a) First Time Photonic Curing. (b) Reorienting the Part and Repulsing on the Partially Cured Areas

Preliminary experimentation with the Novacentrix Metalon ICI-021 ink on Wausau 110 lb paper samples have revealed promising results. A printed coupon (Section 3.1) at a 45˚

slope orientation gave a high resistance value of 10.9 Ω when photonically cured using the optimized curing parameters (Table 3). The high resistance value obtained was due to the partial curing of the printed ink, which signifies that only the top layer of the ink is cured and not through the full thickness. Reorienting the same coupon to a 0˚ slope configuration and repulsing using the optimized parameters resulted in a resistance value of 1.8 Ω, which is comparable to those of fully cured samples. Thus, the process of repulsing on partially cured inks should be a good area for future investigation.

Simpulse® is a thermal simulation software from Novacentrix, which is used to predict the temperature profiles of printed inks undergoing photonic curing. Simpulse® simulation of the partially cured copper oxide ink on paper substrate revealed that for the same power density, the surface temperature of the printed ink lowers with the increase in the thickness of the partially cured copper layer (Figure 43). Thus, in order to attain the optimal curing temperature during repulsing of partially cured samples, a relative higher power density is required compared to uncured samples.

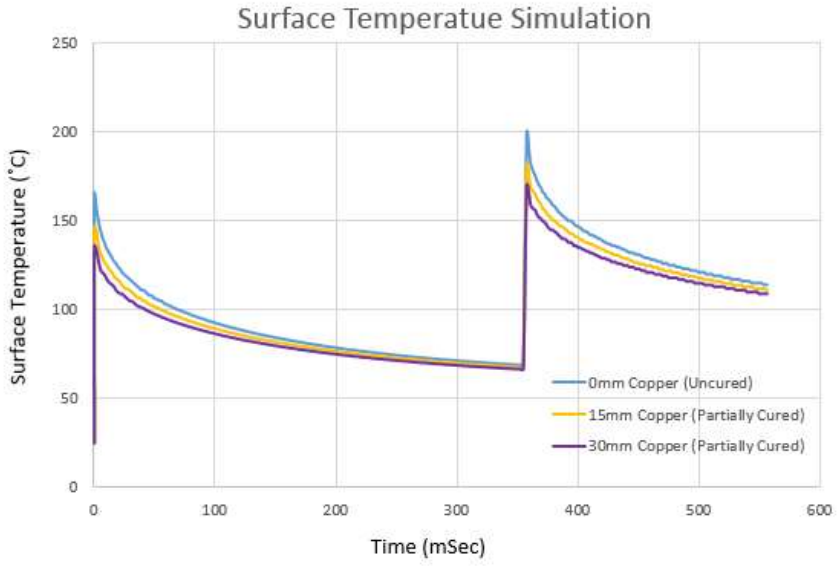

Figure 43: Surface Temperature Simulation (Simpulse®)

A Thermogravimetric analysis (TGA) can be used to determine the temperature at which the uncured copper oxide reacts with the reducing agent to form copper. Also, a TGA can be used to determine the temperature at which the cured copper oxidizes. Thus from the aforementioned experiments, we can determine the temperature window necessary for the proper curing of the copper oxide ink. Later, Simpulse® can be used to determine the machine parameters required for attaining the temperature settings for the photonic curing process.

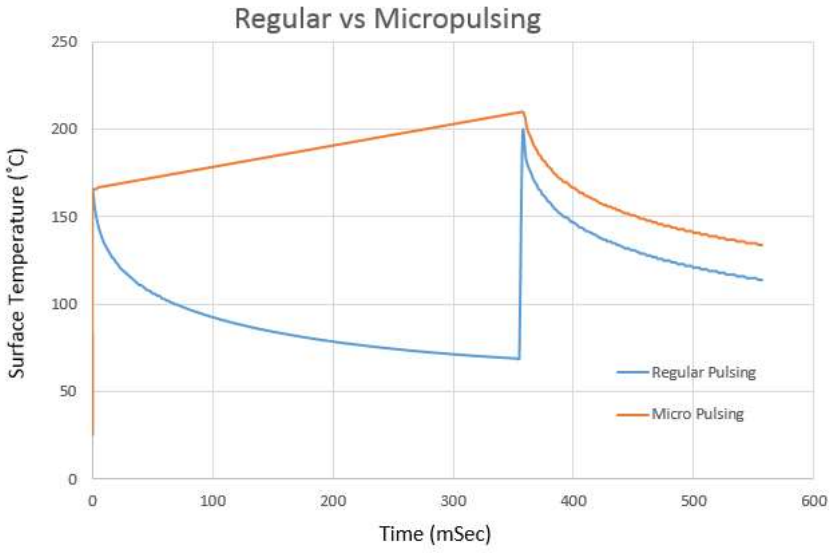

Figure 44: Ink Surface Temperature Profiles of Regular vs Micro-pulsing

However, one of the main problems associated with regular photonic pulsing are huge thermal shocks on the printed ink during each pulse cycle (Figure 44). This is not desired as it causes the printed ink to blow-off and degrade its electrical properties. The micro-pulsing settings in the Novacentrix Pulse Forge 3300 appear to be a promising approach that can lessen the effects of these thermal shocks. Micro-pulsing simply means breaking a regular photonic pulse into multiple smaller pulses while keeping the total power density

to be the same. This process helps in maintaining a constant surface temperature of the printed ink throughout the photonic curing process, thus lessening thermal shock (Figure 44). The Simpulse software can be used to determine the micro-pulse parameters as well. Moreover, simulated experiments can be conducted using Simpulse to develop a temperature step function which will help us identify the micro-pulse parameters for any ink-substrate combination.

References

[1] K. Church, et al., "Printed electronic processes for flexible hybrid circuits and antennas," in Flexible Electronics & Displays Conference and Exhibition, 2009., 2009, pp. 1-7.

[2] M. A. Islam, H. N. Hansen, and P. T. Tang, "Micro-MID Manufacturing By Two-Shot Injection Moulding," OnBoard Technology, vol. 9, pp. 10-13, 2008.

[3] D. Gries, "Laser direct structuring creates low-cost 3D integrated circuits," Laser focus world, vol. 46, pp. 59-63, 2010.

[4] I. Gibson, D. W. Rosen, and B. Strucker. (2013, Additive Manufacturing Technologies - Springer. Available: http://link.springer.com/book/10.1007/978-1-4419-1120-9/page/1

[5] W. Gao, et al., "The status, challenges, and future of additive manufacturing in engineering," Computer-Aided Design. v 69, p 65-89, December 1, 2015

[6] J. Hu, "Overview of flexible electronics from ITRI's viewpoint," in VLSI Test Symposium (VTS), 2010 28th, 2010, pp. 84-84.

[7] K. K. B. Hon, L. Li, and I. M. Hutchings, "Direct writing technology-Advances and developments," CIRP Annals - Manufacturing Technology, vol. 57, pp. 601-620, 2008.

[8] J. Mei, M. R. Lovell, and M. H. Mickle, "Formulation and processing of novel conductive solution inks in continuous inkjet printing of 3-D electric circuits," Electronics Packaging Manufacturing, IEEE Transactions on, vol. 28, pp. 265-273, 2005.

[9] T. Blumenthal, V. Fratello, G. Nino, and K. Ritala, "Conformal printing of sensors on 3D and flexible surfaces using aerosol jet deposition," in SPIE Smart

Structures and Materials+ Nondestructive Evaluation and Health Monitoring, 2013, pp. 86910P-86910P-9.

[10] A. Kamyshny, J. Steinke, and S. Magdassi, "Metal-based inkjet inks for printed electronics," Open Applied Physics Journal, vol. 4, pp. 19-36, 2011.

[11] J. Perelaer, B. J. de Gans, and U. S. Schubert, "Ink-jet Printing and Microwave Sintering of Conductive Silver Tracks," Advanced materials, vol. 18, pp. 2101-2104, 2006.

[12] T. Kumpulainen, J. Pekkanen, J. Valkama, J. Laakso, R. Tuokko, and M. Mäntysalo, "Low temperature nanoparticle sintering with continuous wave and pulse lasers," Optics & Laser Technology, vol. 43, pp. 570-576, 4// 2011.

[13] M. Hummelgård, R. Zhang, H.-E. Nilsson, and H. Olin, "Electrical sintering of silver nanoparticle ink studied by in-situ TEM probing," PloS one, vol. 6, p. e17209, 2011.

[14] K. Schroder, S. McCool, and W. Furlan, "Broadcast Photonic Curing of Metallic Nanoparticle Films," Presented at NSTI Nanotech May, vol. 7, p. 11, 2006.

[15] P. KB and W. CB, "Combining additive manufacturing and direct write for integrated electronics—a review," ed. 24th International Solid Freeform Fabrication Symposium—An Additive Manufacturing Conference, Austin, TX, United states, August 2013, pp. 962–979.

[16] B. K. Park, D. Kim, S. Jeong, J. Moon, and J. S. Kim, "Direct writing of copper conductive patterns by ink-jet printing," Thin Solid Films, vol. 515, pp. 7706-7711, 7/16/ 2007.

[17] J. S. Kang, H. S. Kim, J. Ryu, H. Thomas Hahn, S. Jang, and J. W. Joung, "Inkjet printed electronics using copper nanoparticle ink," Journal of Materials Science: Materials in Electronics, vol. 21, pp. 1213-1220, 2010.

[18] F. Medina, et al., "Hybrid manufacturing: Integrating direct write and stereolithography," in 16th Solid Freeform Fabrication Symposium, SFF 2005, August 1, 2005 - August 3, 2005, Austin, TX, United states, 2005, pp. 39-49.

[19] J. Perelaer, M. Klokkenburg, C. E. Hendriks, and U. S. Schubert, "Microwave Flash Sintering of Inkjet-Printed Silver Tracks on Polymer Substrates," Advanced Materials, vol. 21, pp. 4830-4834, 2009.

[20] D. Sourav, C. Denis, and W. Scott, "Potential for Multi-Functional Additive Manufacturing Using Pulsed Photonic Sintering," vol. 43, ed. North American Manufacturing Research Institution Conference, 2015, pp. 1 - 12.

[21] M. Hösel and F. C. Krebs, "Large-scale roll-to-roll photonic sintering of flexo printed silver nanoparticle electrodes," Journal of Materials Chemistry, vol. 22, pp. 15683-15688, 2012.

[22] S. H. Eom, et al., "Polymer solar cells based on inkjet-printed PEDOT:PSS layer," Organic Electronics, vol. 10, pp. 536-542, 5// 2009.

[23] B. Thompson and H. S. Yoon, "Aerosol-Printed Strain Sensor Using PEDOT:PSS," Sensors Journal, IEEE, vol. 13, pp. 4256-4263, 2013.

[24] L. Taoran, V. Lakafosis, L. Ziyin, C. P. Wong, and M. M. Tentzeris, "Inkjet-printed graphene-based wireless gas sensor modules," in Electronic Components and Technology Conference (ECTC), 2012 IEEE 62nd, 2012, pp. 1003-1008.

[25] L. Huang, et al., "Graphene-based conducting inks for direct inkjet printing of flexible conductive patterns and their applications in electric circuits and chemical sensors," Nano Research, vol. 4, pp. 675-684, 2013.

[26] G. Cummins and M. P. Desmulliez, "Inkjet printing of conductive materials: a review," Circuit World, vol. 38, pp. 193-213, 2012.

[27] W. Luo, W. Hu, and S. Xiao, "Size effect on the thermodynamic properties of silver nanoparticles," The Journal of Physical Chemistry C, vol. 112, pp. 2359-2369, 2008.

[28] W. Cui, W. Lu, Y. Zhang, G. Lin, T. Wei, and L. Jiang, "Gold nanoparticle ink suitable for electric-conductive pattern fabrication using in ink-jet printing technology," Colloids and Surfaces A: Physicochemical and Engineering Aspects, vol. 358, pp. 35-41, 4/5/ 2010.

[29] J. Kang, J. Ryu, H. Kim, and H. Hahn, "Sintering of inkjet-printed silver nanoparticles at room temperature using intense pulsed light," Journal of electronic materials, vol. 40, pp. 2268-2277, 2011.

[30] B. Salam, W. L. Lai, L. C. W. Albert, and L. B. Keng, "Low temperature processing of copper conductive ink for printed electronics applications," in Electronics Packaging Technology Conference (EPTC), 2011 IEEE 13th, 2011, pp. 251-255.

[31] J. Zhang, "Sintering of solution-based aluminum nano-particles by laser ignition," in Laser Applications in Microelectronic and Optoelectronic Manufacturing (LAMOM) XVIII, February 4, 2013 - February 7, 2013, San Francisco, CA, United states, 2013, pp. The Society of Photo-Optical Instrumentation Engineers (SPIE).

[32] R. Faddoul, N. Reverdy-Bruas, and A. Blayo, "Formulation and screen printing of water based conductive flake silver pastes onto green ceramic tapes for electronic applications," Materials Science and Engineering: B, vol. 177, pp. 1053-1066, 8/1/ 2012.

[33] E. Halonen, K. Kaija, M. Mantysalo, A. Kemppainen, R. Osterbacka, and N. Bjorklund, "Evaluation of printed electronics manufacturing line with sensor

platform application," in Microelectronics and Packaging Conference, 2009. EMPC 2009. European, 2009, pp. 1-8.

[34] E. Hrehorova, et al., "Gravure Printing of Conductive Inks on Glass Substrates for Applications in Printed Electronics," Display Technology, Journal of, vol. 7, pp. 318-324, 2011.

[35] D. Sung, A. de la Fuente Vornbrock, and V. Subramanian, "Scaling and Optimization of Gravure-Printed Silver Nanoparticle Lines for Printed Electronics," Components and Packaging Technologies, IEEE Transactions on, vol. 33, pp. 105-114, 2010.

[36] T.-M. Lee, J.-H. Noh, I. Kim, D.-S. Kim, and S. Chun, "Reliability of gravure offset printing under various printing conditions," Journal of Applied Physics, vol. 108, pp. 102802-102802-6, 2010.

[37] T.-M. Lee, J.-H. Noh, C. H. Kim, J. Jo, and D.-S. Kim, "Development of a gravure offset printing system for the printing electrodes of flat panel display," Thin Solid Films, vol. 518, pp. 3355-3359, 4/2/ 2010.

[38] A. Datar, "Micro-extrusion Process Parameter Modeling," Rochester Institute of Technology, 2012.

[39] A. Hudd, "Inkjet printing technologies," The Chemistry of Inkjet Inks. New Jersey-London-Singapore: World Scientific, pp. 3-18, 2010.

[40] M. Maiwald, C. Werner, V. Zollmer, and M. Busse, "INKtelligent printing for sensorial applications," Sensor Review, vol. 30, pp. 19-23, / 2010.

[41] J. West, M. Carter, S. Smith, J. Sears, and S. Rapid City, "Photonic Curing of Silver Nanoparticle Based Inks," South Dakota School of Mines and Technology, Rapid City, 2011.

[42] K. A. Schroder, "Mechanisms of photonic curing: Processing high temperature films on low temperature substrates," in Nanotechnology 2011: Electronics, Devices, Fabrication, MEMS, Fluidics and Computational - 2011 NSTI Nanotechnology Conference and Expo, NSTI-Nanotech 2011, June 13, 2011 - June 16, 2011, Boston, MA, United states, 2011, pp. 220-223.

[43] L. Makkonen, "On the Methods To Determine Surface Energies," Langmuir, vol. 16, pp. 7669-7672, 2000/10/01 2000.

[44] E. Halonen, T. Viiru, K. Ostman, A. L. Cabezas, and M. Mantysalo, "Oven Sintering Process Optimization for Inkjet-Printed Ag Nanoparticle Ink," IEEE Transactions on Components, Packaging and Manufacturing Technology, vol. 3, pp. 350-6, 02/ 2013.

[45] D. Roberson, R. Wicker, and E. MacDonald, "Ohmic curing of printed silver conductive traces," Journal of Electronic Materials, vol. 41, pp. 2553-2566, 2012.

Appendix

Appendix A

Standard Order	Run Order	Blocks	Voltage (V)	Pulse Length (µsec)	Frequency (Hz)	Resistance (Ω)
10	1	1	275	1350	3	1.3
1	2	1	265	1300	2.5	1.6
9	3	1	265	1350	3	1.8
17	4	1	270	1350	3	1.6
13	5	1	270	1350	2.5	1.7
2	6	1	275	1300	2.5	1.5
19	7	1	270	1350	3	1.7
12	8	1	270	1400	3	1.8
20	9	1	270	1350	3	1.5
4	10	1	275	1400	2.5	1.4
18	11	1	270	1350	3	1.6
6	12	1	275	1300	3.5	1.6
15	13	1	270	1350	3	1.6
7	14	1	265	1400	3.5	1.7
16	15	1	270	1350	3	1.6
11	16	1	270	1300	3	1.6
8	17	1	275	1400	3.5	1.6
3	18	1	265	1400	2.5	1.8
5	19	1	265	1300	3.5	1.9
14	20	1	270	1350	3.5	1.8
42	21	3	275	1300	2.5	2.1
56	22	3	270	1350	3	1.5
47	23	3	265	1400	3.5	2.2
49	24	3	265	1350	3	1.8
44	25	3	275	1400	2.5	1.4
43	26	3	265	1400	2.5	1.7
45	27	3	265	1300	3.5	1.9
55	28	3	270	1350	3	1.6
46	29	3	275	1300	3.5	1.8
41	30	3	265	1300	2.5	1.7
51	31	3	270	1300	3	1.7
60	32	3	270	1350	3	1.6
57	33	3	270	1350	3	1.7
53	34	3	270	1350	2.5	1.7
59	35	3	270	1350	3	1.7

54	36	3	270	1350	3.5	1.6
52	37	3	270	1400	3	1.9
48	38	3	275	1400	3.5	1.7
50	39	3	275	1350	3	1.4
58	40	3	270	1350	3	1.7
23	41	2	265	1400	2.5	1.8
26	42	2	275	1300	3.5	1.5
30	43	2	275	1350	3	1.9
22	44	2	275	1300	2.5	1.8
27	45	2	265	1400	3.5	1.8
24	46	2	275	1400	2.5	1.8
36	47	2	270	1350	3	1.7
25	48	2	265	1300	3.5	1.8
31	49	2	270	1300	3	1.6
21	50	2	265	1300	2.5	2
28	51	2	275	1400	3.5	1.9
35	52	2	270	1350	3	1.6
34	53	2	270	1350	3.5	1.6
32	54	2	270	1400	3	1.4
29	55	2	265	1350	3	1.7
40	56	2	270	1350	3	1.7
38	57	2	270	1350	3	1.6
37	58	2	270	1350	3	1.6
33	59	2	270	1350	2.5	1.6
39	60	2	270	1350	3	1.6

Appendix B

Response Surface Regression

Analysis of Variance

Source	DF	Adj SS	Adj MS	F-Value	P-Value
Model	5	0.31000	0.062000	2.49	0.042
Blocks	2	0.07900	0.039500	1.58	0.215
Linear	3	0.23100	0.077000	3.09	0.035
Voltage	1	0.20833	0.208333	8.35	0.006
Pulse Length	1	0.00133	0.001333	0.05	0.818
Frequency	1	0.02133	0.021333	0.86	0.359
Error	54	1.34650	0.024935		
Lack-of-Fit	39	1.27983	0.032816	7.38	0.000
Pure Error	15	0.06667	0.004444		
Total	59	1.65650			

Model Summary

S	R-sq	R-sq(adj)	R-sq(pred)
0.157909	18.71%	11.19%	0.00%

Appendix C

Standard Order	Run Order	Blocks	Distance (mm)	Slope (degree)	Resistance (Ω)
8	1	1	20	45	3.1
16	2	1	30	45	5.3
11	3	1	25	30	2.2
13	4	1	30	0	2
6	5	1	20	15	1.9
5	6	1	20	0	1.9
15	7	1	30	30	3
10	8	1	25	15	2
14	9	1	30	15	2.4
9	10	1	25	0	2
2	11	1	15	15	1.8
7	12	1	20	30	2
1	13	1	15	0	1.8
4	14	1	15	45	2.7
3	15	1	15	30	1.8
12	16	1	25	45	3.2
27	17	2	25	30	2.4
23	18	2	20	30	2.1
17	19	2	15	0	2.1
20	20	2	15	45	2.6
22	21	2	20	15	1.6
29	22	2	30	0	2.1
19	23	2	15	30	1.8
18	24	2	15	15	1.9
25	25	2	25	0	2.2
30	26	2	30	15	2.4
32	27	2	30	45	5.5
24	28	2	20	45	3.1
26	29	2	25	15	2
28	30	2	25	45	3.9
21	31	2	20	0	2.2
31	32	2	30	30	2.8
74	33	5	25	15	1.8
69	34	5	20	0	2.4
75	35	5	25	30	2.4
66	36	5	15	15	2.3
70	37	5	20	15	1.8
80	38	5	30	45	5.5

73	39	5	25	0	2
78	40	5	30	15	2.3
67	41	5	15	30	1.9
79	42	5	30	30	3.1
72	43	5	20	45	3.2
71	44	5	20	30	2.3
68	45	5	15	45	2.9
76	46	5	25	45	4.3
77	47	5	30	0	2.1
65	48	5	15	0	2.1
56	49	4	20	45	3.3
61	50	4	30	0	2.1
64	51	4	30	45	5.6
63	52	4	30	30	3
54	53	4	20	15	1.7
59	54	4	25	30	2.5
52	55	4	15	45	2.8
62	56	4	30	15	2.4
57	57	4	25	0	1.8
49	58	4	15	0	1.6
60	59	4	25	45	3.4
51	60	4	15	30	1.8
53	61	4	20	0	1.4
55	62	4	20	30	2.5
50	63	4	15	15	1.9
58	64	4	25	15	1.8
42	65	3	25	15	1.9
43	66	3	25	30	2.5
46	67	3	30	15	2.4
36	68	3	15	45	2.8
38	69	3	20	15	1.6
37	70	3	20	0	1.7
45	71	3	30	0	2.2
40	72	3	20	45	3.2
34	73	3	15	15	1.8
48	74	3	30	45	5.7
39	75	3	20	30	2.1
47	76	3	30	30	3.1
41	77	3	25	0	2.4
33	78	3	15	0	2.5
44	79	3	25	45	3.4
35	80	3	15	30	2

Appendix D

Multilevel Factorial Design

```
Factors:       2     Replicates:     5
Base runs:    16     Total runs:    80
Base blocks:   1     Total blocks:   5

Number of levels: 4, 4
```

General Linear Model: Resistance versus Blocks, Distance, Slope

```
Factor    Type   Levels  Values
Blocks    fixed       5  1, 2, 3, 4, 5
Distance  fixed       4  15, 20, 25, 30
Slope     fixed       4  0, 15, 30, 45


Analysis of Variance for Resistance, using Adjusted SS for Tests

Source          DF   Seq SS   Adj SS   Adj MS       F      P
Blocks           4   0.4368   0.4368   0.1092    2.66  0.041
Distance         3  14.8514  14.8514   4.9505  120.39  0.000
Slope            3  42.4794  42.4794  14.1598  344.35  0.000
Distance*Slope   9  12.0951  12.0951   1.3439   32.68  0.000
Error           60   2.4673   2.4673   0.0411
Total           79  72.3299


S = 0.202783   R-Sq = 96.59%   R-Sq(adj) = 95.51%


Unusual Observations for Resistance

Obs  Resistance      Fit   SE Fit  Residual  St Resid
 34     2.40000  2.03125  0.10139   0.36875      2.10 R
 46     4.30000  3.75125  0.10139   0.54875      3.12 R
 58     1.60000  1.95625  0.10139  -0.35625     -2.03 R
 61     1.40000  1.85625  0.10139  -0.45625     -2.60 R
 62     2.50000  2.13625  0.10139   0.36375      2.07 R
 78     2.50000  2.06250  0.10139   0.43750      2.49 R

R denotes an observation with a large standardized residual.
```

Appendix E

Standard Order	Run Order	Blocks	Distance (mm)	Position	Mean Energy Density (J/cm^2)
60	1	3	30	5	4.308
55	2	3	25	5	4.605
53	3	3	25	3	3.979
43	4	3	15	3	4.624
57	5	3	30	2	3.115
59	6	3	30	4	3.986
46	7	3	20	1	4.194
48	8	3	20	3	4.025
49	9	3	20	4	4.569
51	10	3	25	1	3.904
42	11	3	15	2	4.718
44	12	3	15	4	4.952
58	13	3	30	3	3.498
52	14	3	25	2	3.651
45	15	3	15	5	5.238
47	16	3	20	2	4.199
54	17	3	25	4	4.362
56	18	3	30	1	3.716
41	19	3	15	1	4.816
50	20	3	20	5	4.921
25	21	2	15	5	5.193
29	22	2	20	4	4.443
33	23	2	25	3	3.839
26	24	2	20	1	4.113
38	25	2	30	3	3.569
30	26	2	20	5	4.953
21	27	2	15	1	4.696
23	28	2	15	3	4.629
24	29	2	15	4	5.003
36	30	2	30	1	3.534
40	31	2	30	5	4.368
28	32	2	20	3	4.188
27	33	2	20	2	3.933
31	34	2	25	1	3.842
39	35	2	30	4	3.936
37	36	2	30	2	3.272
35	37	2	25	5	4.716
22	38	2	15	2	4.704

32	39	2	25	2	3.719
34	40	2	25	4	4.261
14	41	1	25	4	4.324
13	42	1	25	3	3.874
19	43	1	30	4	3.934
5	44	1	15	5	5.307
12	45	1	25	2	3.844
17	46	1	30	2	3.312
10	47	1	20	5	4.945
2	48	1	15	2	4.603
3	49	1	15	3	4.642
1	50	1	15	1	4.862
15	51	1	25	5	4.662
20	52	1	30	5	4.333
9	53	1	20	4	4.466
8	54	1	20	3	4.272
16	55	1	30	1	3.668
11	56	1	25	1	4.072
4	57	1	15	4	4.932
6	58	1	20	1	4.271
7	59	1	20	2	4.083
18	60	1	30	3	3.375
76	61	4	30	1	3.766
68	62	4	20	3	4.21
72	63	4	25	2	3.555
62	64	4	15	2	4.663
65	65	4	15	5	5.253
74	66	4	25	4	4.317
75	67	4	25	5	4.653
63	68	4	15	3	4.795
77	69	4	30	2	3.396
73	70	4	25	3	3.98
61	71	4	15	1	4.847
70	72	4	20	5	4.903
69	73	4	20	4	4.598
67	74	4	20	2	3.997
71	75	4	25	1	4.046
79	76	4	30	4	3.974
80	77	4	30	5	4.252
64	78	4	15	4	5.081
66	79	4	20	1	4.253
78	80	4	30	3	3.403

81	81	5	15	1	4.908
84	82	5	15	4	4.984
89	83	5	20	4	4.425
85	84	5	15	5	5.281
88	85	5	20	3	4.287
93	86	5	25	3	3.992
92	87	5	25	2	3.652
87	88	5	20	2	3.964
95	89	5	25	5	4.592
94	90	5	25	4	4.277
91	91	5	25	1	4.052
82	92	5	15	2	4.547
100	93	5	30	5	4.291
90	94	5	20	5	4.931
86	95	5	20	1	4.39
97	96	5	30	2	3.213
96	97	5	30	1	3.654
99	98	5	30	4	3.938
98	99	5	30	3	3.604
83	100	5	15	3	4.778

Appendix F

General Linear Model: Mean versus Blocks, Distance, Position

```
Factor    Type   Levels  Values
Blocks    fixed       5  1, 2, 3, 4, 5
Distance  fixed       4  15, 20, 25, 30
Position  fixed       5  1, 2, 3, 4, 5


Analysis of Variance for Mean, using Adjusted SS for Tests

Source             DF   Seq SS   Adj SS  Adj MS       F      P
Blocks              4   0.0344   0.0344  0.0086    1.40  0.243
Distance            3  17.4213  17.4213  5.8071  942.51  0.000
Position            4   9.4016   9.4016  2.3504  381.48  0.000
Distance*Position  12   0.3759   0.3759  0.0313    5.08  0.000
Error              76   0.4683   0.4683  0.0062
Total              99  27.7015


S = 0.0784939   R-Sq = 98.31%   R-Sq(adj) = 97.80%
```

Appendix G

Angle (Degree)	Light Intensity (J/cm^2)
45	3.486
30	4.189
30	4.169
0	4.896
15	4.682
30	4.166
30	4.172
45	3.477
0	4.904
15	4.682
0	4.902
15	4.669
30	4.179
15	4.706
0	4.891
45	3.538
0	4.896
45	3.48
0	4.855
30	4.156
0	4.865
45	3.478
45	3.432
30	4.21
15	4.684
45	3.456
30	4.168
45	3.521
15	4.688
45	3.509
15	4.697
0	4.887
15	4.694
15	4.704
0	4.871
30	4.166
30	4.17
45	3.482
0	4.898
15	4.693

Appendix H

One-way ANOVA: Light Intensity versus Angle

```
Method

Null hypothesis         All means are equal
Alternative hypothesis  At least one mean is different
Significance level      α = 0.05

Equal variances were assumed for the analysis.


Factor Information

Factor  Levels  Values
Angle        4  0, 15, 30, 45


Analysis of Variance

Source  DF   Adj SS   Adj MS  F-Value  P-Value
Angle    3  11.7417  3.91392  9883.07    0.000
Error   36   0.0143  0.00040
Total   39  11.7560
```

Appendix I

Incident angle	Receiving angle	X	Y	Z	x	y	L*	a*	b*	C*ab	h*ab
60	-40	2.48	2.57	2.81	0.3158	0.3268	18.23	0.81	-0.07	0.81	355.08
45	-25	2.82	2.95	3.27	0.3123	0.3264	19.85	0.34	-0.33	0.47	315.42
30	-10	4.55	4.77	5.52	0.3067	0.3214	26.07	0.23	-1.47	1.49	278.74
15	5	29.49	30.96	29.53	0.3277	0.3441	62.47	0.24	5.86	5.87	87.7
15	7	38.09	39.92	36.9	0.3315	0.3474	69.42	0.46	7.85	7.87	86.63
15	9	52.65	55.08	48.9	0.3362	0.3516	79.08	0.78	10.81	10.84	85.86
15	11	74.62	77.75	65.63	0.3423	0.3567	90.67	1.47	14.99	15.07	84.39
30	-5	5.37	5.66	6.47	0.3069	0.3233	28.53	-0.09	-1.25	1.26	266.04
45	-20	2.97	3.07	3.54	0.3096	0.3204	20.32	0.86	-1.23	1.5	304.89
60	-35	2.5	2.59	2.83	0.3158	0.3265	18.31	0.86	-0.11	0.87	352.73
60	-30	2.49	2.6	2.79	0.3158	0.3301	18.37	0.31	0.31	0.44	44.3
45	-15	3.14	3.26	3.8	0.3078	0.3199	21.07	0.65	-1.43	1.57	294.58
30	0	6.68	7.03	7.94	0.3085	0.3248	31.87	-0.05	-0.99	0.99	267.03
15	13	107.99	111.41	85.4	0.3543	0.3655	104.25	3.39	22.92	23.17	81.59
15	15	161.26	163.26	111.09	0.3702	0.3748	120.59	7.58	34.19	35.02	77.5
15	17	145.1	148.08	105.53	0.3639	0.3714	116.22	5.81	30.07	30.62	79.07
15	19	106.26	110.27	88.74	0.3481	0.3612	103.84	2.37	19.84	19.98	83.19
30	5	8.63	9.08	9.99	0.3115	0.3279	36.14	-0.05	-0.29	0.29	260.5
45	-10	3.36	3.51	4.06	0.3072	0.3215	22	0.28	-1.29	1.32	282.33
60	-25	2.57	2.66	2.97	0.3132	0.3243	18.61	0.8	-0.52	0.95	327.02
60	-20	2.63	2.74	3.07	0.3119	0.3246	18.98	0.53	-0.55	0.77	313.85
45	-5	3.67	3.83	4.48	0.3062	0.3198	23.11	0.42	-1.62	1.67	284.62

30	10	12.33	12.98	13.71	0.3161	0.3327	42.74	-0.04	1.05	1.05	92.04
15	21	67.19	70.14	60.94	0.3389	0.3538	87.07	1.13	12.91	12.96	85
15	23	50.08	52.44	47.48	0.3339	0.3496	77.54	0.64	9.64	9.66	86.2
15	25	38.19	40.05	37.44	0.3301	0.3462	69.5	0.4	7.32	7.33	86.88
15	30	21.63	22.73	22.65	0.3228	0.3392	54.79	0.13	3.58	3.58	87.84
30	15	19.42	20.4	20.56	0.3216	0.3379	52.29	0.13	3.01	3.02	87.62
45	0	4.08	4.29	4.97	0.3057	0.3217	24.61	-0.02	-1.44	1.44	269.26
60	-15	2.7	2.83	3.19	0.3099	0.3245	19.35	0.24	-0.69	0.73	289.3
60	-10	2.82	2.96	3.33	0.3095	0.3249	19.89	0.1	-0.67	0.68	278.4
45	5	4.82	5.05	5.88	0.3059	0.3209	26.89	0.18	-1.63	1.64	276.47
30	20	34.97	36.64	34.75	0.3288	0.3445	67.01	0.47	6.46	6.48	85.82
15	35	14.01	14.74	15.4	0.3173	0.3338	45.27	0	1.45	1.45	90.02
15	40	10.2	10.73	11.61	0.3135	0.3297	39.12	0.01	0.21	0.21	86.38
30	22	47.25	49.46	45.41	0.3325	0.348	75.74	0.66	8.76	8.79	85.68
30	24	64.92	67.85	60.36	0.3361	0.3513	85.93	0.96	11.47	11.51	85.21
45	10	5.71	6.02	6.89	0.3068	0.3232	29.46	-0.09	-1.31	1.31	265.89
60	-5	2.98	3.12	3.59	0.3072	0.3221	20.52	0.17	-1.16	1.18	278.31
60	0	3.22	3.39	3.9	0.3064	0.3227	21.56	-0.07	-1.17	1.17	266.69
45	15	7.48	7.87	8.77	0.31	0.3263	33.71	-0.03	-0.66	0.66	267.57
30	30	254.37	257	172.85	0.3718	0.3756	142.89	9.3	40.68	41.73	77.13
30	28	149.85	154.61	119.6	0.3534	0.3646	118.13	3.76	24.94	25.22	81.43
30	26	103.71	107.94	90.71	0.343	0.357	102.99	1.85	17	17.1	83.79
15	45	7.86	8.27	9.18	0.3104	0.3269	34.55	-0.07	-0.54	0.55	262.52
15	50	6.27	6.59	7.53	0.3074	0.3233	30.85	0.02	-1.29	1.29	270.81
30	34	136.94	142.26	117.33	0.3454	0.3588	114.46	2.37	19.93	20.07	83.21
30	32	192.77	197.76	146.62	0.3589	0.3682	129.6	5.29	30.22	30.68	80.07
45	20	10.23	10.74	11.61	0.314	0.3297	39.15	0.15	0.25	0.29	59.64

60	5	3.52	3.7	4.29	0.3061	0.3213	22.65	0.12	-1.4	1.41	274.77
60	10	3.93	4.12	4.83	0.3053	0.3198	24.07	0.25	-1.71	1.73	278.29
45	25	15.46	16.21	16.79	0.319	0.3345	47.26	0.29	1.82	1.84	80.91
30	40	48.96	51.25	47.84	0.3307	0.3462	76.83	0.66	8.03	8.06	85.31
30	38	64.1	67.01	60.91	0.3338	0.349	85.51	0.92	10.25	10.29	84.87
30	36	91.44	95.39	83.21	0.3386	0.3532	98.19	1.4	14.06	14.13	84.32
15	55	5.22	5.48	6.38	0.3059	0.3207	28.05	0.21	-1.71	1.72	277.14
15	60	4.49	4.72	5.5	0.3054	0.321	25.93	0.05	-1.61	1.61	271.88
30	45	28.77	30.15	29.49	0.3254	0.341	61.79	0.44	4.73	4.75	84.72
45	30	25.22	26.43	26.15	0.3242	0.3398	58.45	0.4	4.06	4.08	84.36
60	15	4.5	4.74	5.47	0.3059	0.3222	25.99	-0.07	-1.41	1.41	267.25
60	20	5.42	5.7	6.55	0.3069	0.3227	28.65	0.03	-1.36	1.36	271.46
45	35	50.87	53.2	49.8	0.3306	0.3457	77.99	0.82	7.98	8.03	84.12
30	50	18.33	19.21	19.6	0.3208	0.3362	50.93	0.38	2.49	2.52	81.43
30	55	13.14	13.8	14.55	0.3168	0.3325	43.94	0.2	1.1	1.12	79.67
45	41	159.46	166.07	143.65	0.3399	0.354	121.37	1.99	17.53	17.64	83.52
45	39	107.45	112.1	99.93	0.3363	0.3509	104.5	1.45	13.44	13.51	83.84
45	37	72.51	75.78	69.34	0.3332	0.3482	89.76	1	10.3	10.35	84.46
60	25	6.91	7.23	8.16	0.3099	0.3242	32.32	0.4	-0.99	1.07	291.78
60	30	9.41	9.87	10.76	0.3132	0.3285	37.6	0.23	-0.04	0.24	351.07
45	45	559.33	567.17	392.59	0.3682	0.3734	190.87	11.01	50.04	51.23	77.59
45	43	298.97	307.92	240.31	0.3529	0.3635	152.76	5.17	30.61	31.05	80.42
30	60	9.68	10.16	11.07	0.3132	0.3288	38.13	0.16	0.01	0.16	3.9
30	65	7.6	7.98	8.88	0.3107	0.3262	33.95	0.15	-0.62	0.63	283.33
45	51	156.92	163.7	146.71	0.3358	0.3503	120.71	1.65	14.85	14.94	83.65
45	49	188.66	196.45	170.14	0.3398	0.3538	129.28	2.15	18.44	18.56	83.35
45	47	336.79	347.34	273.46	0.3517	0.3627	159.67	5.04	31.08	31.48	80.79

60	35	14.09	14.75	15.42	0.3183	0.3333	45.29	0.42	1.44	1.5	73.69
60	40	22.96	24.02	24.19	0.3226	0.3375	56.1	0.59	3.2	3.26	79.55
45	55	78.83	82.41	77.93	0.3296	0.3446	92.76	0.98	8.64	8.69	83.54
45	53	101.68	106.23	98.57	0.3318	0.3466	102.36	1.18	10.63	10.69	83.67
45	60	46.29	48.4	47.3	0.326	0.3409	75.08	0.81	5.58	5.64	81.77
60	45	42.02	43.88	42.95	0.3261	0.3405	72.15	0.94	5.32	5.4	79.94
60	50	88.07	92.06	88.42	0.3279	0.3428	96.85	1.04	8	8.07	82.58
45	65	28.65	29.96	30.22	0.3225	0.3373	61.62	0.68	3.39	3.45	78.61
45	70	20.22	21.12	21.84	0.32	0.3343	53.08	0.7	2.05	2.16	71.21
60	52	137.11	143.21	136.28	0.3291	0.3438	114.75	1.35	9.93	10.03	82.27
60	54	163.64	171.07	162.37	0.3292	0.3441	122.73	1.27	10.74	10.81	83.27
60	56	266.88	278.92	261.97	0.3304	0.3453	147.29	1.55	13.58	13.67	83.47
60	58	614.79	639.44	571	0.3368	0.3503	199.31	3.54	23.8	24.06	81.55
60	60	1077.89	1108.16	873.62	0.3523	0.3622	242.62	8.59	45.57	46.37	79.32
60	62	987.55	1025.58	889.48	0.3402	0.3533	236.03	4.7	31.8	32.14	81.59
60	64	443.42	463.97	446.4	0.3275	0.3427	177.47	1.51	13.53	13.61	83.63
60	66	253.45	265.73	264.44	0.3234	0.3391	144.67	0.79	8.23	8.26	84.53
60	68	178.42	187.1	188.66	0.322	0.3376	126.94	0.66	6.27	6.31	83.98
60	70	132.71	139.05	141.78	0.3209	0.3362	113.47	0.76	4.87	4.93	81.14
60	75	93.16	97.45	100.84	0.3196	0.3344	99	0.95	3.37	3.5	74.3
45	-65	2.46	2.56	2.76	0.3161	0.3292	18.17	0.5	0.21	0.54	22.71
30	-50	2.59	2.69	3.02	0.3124	0.3238	18.74	0.76	-0.62	0.98	320.57
15	-35	3.54	3.71	4.29	0.307	0.3213	22.68	0.28	-1.35	1.37	281.68
15	-40	3.28	3.42	3.98	0.307	0.3203	21.65	0.45	-1.44	1.51	287.28
30	-55	2.54	2.64	2.93	0.3134	0.3259	18.56	0.58	-0.31	0.66	331.59
45	-70	2.37	2.47	2.68	0.3155	0.3281	17.78	0.55	0.06	0.55	5.92
30	-60	2.47	2.57	2.86	0.3127	0.3255	18.24	0.52	-0.4	0.66	322.68

15	-45	3.03	3.17	3.63	0.3084	0.3223	20.71	0.34	-1.07	1.12	287.45
15	-50	2.91	3.04	3.49	0.3081	0.3223	20.21	0.3	-1.08	1.12	285.68
30	-65	2.39	2.48	2.81	0.3116	0.323	17.84	0.72	-0.74	1.03	314.08
15	-55	2.74	2.86	3.3	0.308	0.3209	19.46	0.49	-1.23	1.33	291.79
15	-60	2.62	2.73	3.15	0.3082	0.3212	18.95	0.48	-1.16	1.26	292.44
75	-75	0	0	0	0	0	0	0	0	0	0
75	-65	0	0	0	0	0	0	0	0	0	0
75	-60	0	0	0	0	0	0	0	0	0	0
75	-55	2.65	2.68	2.92	0.3209	0.325	18.72	1.92	-0.01	1.92	359.8
75	-50	2.69	2.77	2.91	0.321	0.3312	19.11	0.98	0.74	1.23	36.86
75	-45	2.52	2.57	2.78	0.3203	0.3264	18.23	1.59	0.12	1.59	4.47
75	-40	2.53	2.66	2.72	0.3199	0.3368	18.65	-0.04	1.31	1.31	91.89
75	-35	2.52	2.66	2.8	0.3162	0.3332	18.62	-0.08	0.68	0.69	96.74
75	-30	2.43	2.55	2.7	0.3167	0.3319	18.15	0.18	0.56	0.58	72.09
75	-25	2.56	2.71	2.86	0.3148	0.3338	18.86	-0.4	0.68	0.79	120.21
75	-20	2.62	2.68	3.05	0.3138	0.321	18.72	1.41	-0.87	1.66	328.18
75	-15	2.5	2.57	3	0.3098	0.3186	18.24	1.13	-1.36	1.77	309.83
75	-10	2.67	2.82	3.1	0.3108	0.3278	19.29	-0.13	-0.24	0.27	241.08
75	-5	2.59	2.75	3.02	0.31	0.329	19.01	-0.44	-0.14	0.46	198.4
75	0	2.77	2.86	3.38	0.3075	0.3174	19.46	0.97	-1.68	1.94	299.96
75	5	2.91	3.03	3.48	0.3087	0.322	20.16	0.46	-1.08	1.17	292.85
75	10	3.03	3.21	3.61	0.3077	0.3257	20.85	-0.32	-0.7	0.77	245.3
75	15	3.43	3.58	4.22	0.3054	0.3187	22.22	0.43	-1.76	1.82	283.83
75	20	3.7	3.92	4.45	0.3066	0.3247	23.39	-0.38	-0.94	1.01	248.11
75	25	4.36	4.59	5.29	0.3061	0.3223	25.53	-0.06	-1.36	1.36	267.38
75	30	5.36	5.61	6.44	0.3079	0.3223	28.41	0.31	-1.34	1.37	283.24
75	35	7.14	7.46	8.34	0.3115	0.325	32.82	0.57	-0.74	0.93	307.8

75	40	10.17	10.62	11.44	0.3157	0.3294	38.93	0.65	0.34	0.73	27.63
75	45	16.18	16.87	17.64	0.3192	0.3328	48.1	0.84	1.51	1.72	61.01
75	50	27.08	28.31	28.9	0.3213	0.3358	60.16	0.7	2.81	2.9	76.03
75	55	47.5	49.58	50.66	0.3215	0.3356	75.81	1.03	3.34	3.5	72.81
75	60	89.75	93.85	96.41	0.3205	0.3352	97.57	0.99	3.8	3.92	75.45
75	65	189.34	198.29	206.68	0.3186	0.3336	129.73	0.95	3.67	3.79	75.45
75	67	218.72	229.4	241.65	0.3171	0.3326	136.99	0.67	2.93	3.01	77.05
75	69	321.05	336.92	357.58	0.3161	0.3318	157.9	0.62	2.6	2.67	76.61
75	71	575.46	604.49	647.74	0.3149	0.3307	195.31	0.46	2	2.05	77.09
75	73	911.27	957.01	1019.35	0.3156	0.3314	230.28	0.62	3.17	3.23	78.88
75	75	5081.54	5323.04	5131.2	0.3271	0.3426	420.36	2.7	30.05	30.18	84.87
0	75	2.57	2.7	3.08	0.3075	0.3235	18.8	0	-0.93	0.93	269.82
0	70	2.8	2.92	3.42	0.3064	0.3194	19.71	0.48	-1.52	1.59	287.48
0	65	2.91	3.05	3.57	0.3054	0.3202	20.25	0.18	-1.49	1.5	276.98
0	60	3.14	3.29	3.86	0.3053	0.3196	21.16	0.26	-1.61	1.63	279
0	55	3.41	3.57	4.21	0.3049	0.3191	22.2	0.29	-1.74	1.77	279.51
0	50	3.73	3.91	4.58	0.3051	0.32	23.38	0.17	-1.67	1.68	275.99
0	45	4.18	4.38	5.14	0.3052	0.32	24.9	0.21	-1.72	1.74	276.8
0	40	4.74	4.99	5.78	0.3057	0.3216	26.69	-0.01	-1.53	1.53	269.64
0	35	5.64	5.94	6.8	0.3069	0.3233	29.27	-0.08	-1.28	1.28	266.24
0	30	6.94	7.3	8.22	0.3088	0.3251	32.49	-0.06	-0.92	0.93	266.28
0	25	8.86	9.34	10.23	0.3116	0.3285	36.63	-0.15	-0.18	0.23	229.81
0	20	12.14	12.78	13.56	0.3155	0.3321	42.43	-0.04	0.89	0.89	92.53
0	15	0	0	0	0	0	0	0	0	0	0
0	-75	2.65	2.79	3.16	0.3086	0.3239	19.17	0.11	-0.83	0.83	277.5
0	-70	2.74	2.87	3.29	0.3074	0.3229	19.53	0.08	-1.02	1.03	274.73
0	-65	2.89	3.01	3.56	0.3051	0.3186	20.1	0.39	-1.71	1.75	282.84

0	-60	3.1	3.25	3.81	0.305	0.3199	21.03	0.17	-1.59	1.6	276.21
0	-55	3.34	3.49	4.15	0.3042	0.3176	21.9	0.43	-1.97	2.01	282.21
0	-50	3.61	3.79	4.44	0.3048	0.3199	22.95	0.14	-1.68	1.69	274.72
0	-45	4.05	4.24	4.98	0.3051	0.3197	24.46	0.22	-1.75	1.76	277.25
0	-40	4.59	4.83	5.6	0.3057	0.3214	26.24	0.05	-1.55	1.55	272.01
0	-35	5.29	5.57	6.39	0.3065	0.3231	28.31	-0.13	-1.32	1.32	264.52
0	-30	6.47	6.82	7.7	0.3083	0.325	31.4	-0.14	-0.97	0.98	261.98
0	-25	8.27	8.71	9.58	0.3114	0.328	35.42	-0.11	-0.27	0.29	248.74
0	-20	11.21	11.79	12.58	0.315	0.3314	40.88	0.01	0.67	0.67	89.05
0	-15	0	0	0	0	0	0	0	0	0	0
60	-40	2.52	2.62	2.8	0.3177	0.3296	18.45	0.69	0.36	0.78	27.55